Stimulation strength controls the rate of initiation but not the molecular organization of TCR-induced signalling

Claire Y. Ma[1], John C. Marioni[2,3,4*], Gillian M. Griffiths[1*], Arianne C. Richard[1,2*]

[1]Cambridge Institute for Medical Research, University of Cambridge, Cambridge, UK
[2]Cancer Research UK Cambridge Institute, University of Cambridge, Cambridge, UK
[3]EMBL-European Bioinformatics Institute, Wellcome Genome Campus, Cambridge, UK
[4]Wellcome Sanger Institute, Wellcome Genome Campus, Cambridge, UK
[*] Co-corresponding authors

Abstract

Millions of naïve T cells with different TCRs may interact with a peptide-MHC ligand, but very few will activate. Remarkably, this fine control is orchestrated using a limited set of intracellular machinery. It remains unclear whether changes in stimulation strength alter the programme of signalling events leading to T cell activation. Using mass cytometry to simultaneously measure multiple signalling pathways during activation of murine $CD8^+$ T cells, we found a programme of distal signalling events that is shared, regardless of the strength of TCR stimulation. Moreover, the relationship between transcription of early response genes *Nr4a1* and *Irf8* and activation of the ribosomal protein S6 is also conserved across stimuli. Instead, we found that stimulation strength dictates the rate with which cells initiate signalling through this network. These data suggest that TCR-induced signalling results in a coordinated activation program, modulated in rate but not organization by stimulation strength.

Introduction

Effector differentiation of a naïve $CD8^+$ T cell begins when its T cell receptor (TCR) recognizes a peptide-MHCI ligand complex. If the interaction is strong enough, a cascade of signalling events follows that allows the naïve T cell to differentiate and expand into a pool of effector cells. Signal transduction downstream of the TCR involves a highly diverse network of post-translational protein modifications that ultimately drive transcriptional, translational, metabolic and cytoskeletal changes in the cell. It is estimated that fewer than 0.01 % of naïve $CD8^+$ T cells can recognize a particular foreign peptide-MHCI complex (Jenkins & Moon, 2012). Despite the diversity of rearranged TCRs on these naïve cells and the extensive range of antigenic peptides that may be presented, the intracellular machinery within each naïve T cell is able to sense the strength of the receptor-ligand interaction and mount an appropriate response.

Previous work has demonstrated that the strength of stimulation a T cell receives upon binding a peptide-MHC ligand complex determines its fate in the thymus and its probability of activating in the periphery. During thymic selection, T cells that weakly recognize self-peptides are retained, while those that strongly recognize self-peptides undergo negative selection and are removed (Daniels et al., 2006; Hogquist et al., 1994; Juang et al., 2010; Prasad et al., 2009). In the periphery, the population response to stimuli of different strengths can vary in speed, magnitude and phenotype (Denton et al., 2011; King et al., 2012; Moreau et al., 2012; Ozga et al., 2016; Palmer et al., 2016; Zehn et al., 2009). Work from our group and others indicates that these observations may be explained by the fact that stimulation strength controls the rate with which individual cells activate

transcriptional and proliferative processes (Hommel & Hodgkin, 2007; Richard et al., 2018). This then raises the question, how does stimulation strength impact signalling downstream of the TCR, and how does this relate to transcriptional activation (R. Balyan et al., 2018)?

Many previous studies have examined signalling mediators and their coordinated network during naïve T cell activation (Kannan et al., 2012; Krishnaswamy et al., 2014; G. Voisinne et al., 2019). Signalling through the TCR (Courtney et al., 2018; Navarro & Cantrell, 2014) begins with LCK and Fyn-mediated tyrosine phosphorylation of ITAM motifs on the invariant CD3 subunits. This creates a high affinity binding site for ZAP70, which, upon phosphorylation and activation, leads to the generation of the LAT-SLP76 signalosome. From here, signalling activates multiple cascades including MAPK (MEK1/2-ERK1/2), PDK1-PI3K, calcium, and NFκB (including IκBα-p65) pathways, each amplified and propagated via a series of phosphorylation events or other post-translational modifications. Signal transduction pathways can be broadly categorized as digital, with distinct 'on' or 'off' outcomes, or analogue, giving rise to a graded response (Conley et al., 2016; Zikherman & Au-Yeung, 2015). In digital signalling, once the threshold for activation is surpassed, an output signal of constant intensity is produced. In analogue signalling, higher intensity of the originating stimulus results in a proportionally higher intensity of the output signal.

Previous work has demonstrated that ligand potency determines the extent of signalling at various proximal and distal nodes (Palmer et al., 2016; Rosette et al., 2001). Studies focused on digital signalling nodes showed that stimulation strength affects the percentage of cells that phosphorylate ERK (Altan-Bonnet & Germain, 2005; J. Das et al., 2009; Tian et al., 2007), PKD2 (Navarro et al., 2014), IκBα and the p65 component of NFκB (Kingeter et al.,

2010). Most of these studies have looked at each signalling molecule separately. It therefore remains unclear how ligand potency affects the coordination of signalling downstream of the TCR in naïve T cells.

TCR-induced responses are rapid and often transient, and responding cell populations can be heterogeneous. Single-cell approaches are therefore well-suited to examining this system. Mass cytometry provides single-cell resolution, uses antibody-mediated measurements that can detect post-translational signalling protein modifications, and can achieve high-dimensionality through simultaneous measurement of up to 40 epitopes (Bandura et al., 2009; Bendall et al., 2011; Lou et al., 2007; Ornatsky et al., 2010) . Previous mass cytometry studies of T cell signalling have demonstrated that small differences in proximal signalling molecules are propagated and amplified in downstream targets (Mingueneau et al., 2014) and that the interplay of 'activatory' versus 'inhibitory' signalling components determines the response of effector T cells to different antigen doses (Wolchinsky et al., 2014).

In this study, we designed a mass cytometry panel probing surface receptors and elements of key signalling pathways (Figure 1) to examine the effect of stimulation strength on naïve $CD8^+$ T cell responses. We used a minimal antigen presentation system to ask how modulating only the strength of the TCR-pMHC interaction affects signalling pathways without the influence of variable costimulatory factors or feedback from other cell types. Our multi-dimensional approach allowed us to determine how ligand potency impacts the synchronization of multiple parallel pathways. Through simultaneous measurement of S6 phosphorylation and early mRNA transcripts, we also examined the concurrent activation of

these markers of translational and transcriptional processes. Our data suggest that the coordination of the TCR-induced signalling pathways that we tested does not vary with stimulation strength. Instead, strength of stimulation determines the rate with which T cells initiate this programme.

Results

Mass cytometry detects active T cell conjugates

We used the OT-I TCR transgenic mouse on a recombination-activating gene (RAG)-deficient background as a model for evaluating the impact of stimulation strength on TCR signalling pathways. In this model, all peripheral $CD8^+$ T cells recognize the ovalbumin peptide SIINFEKL. Variants of SIINFEKL with altered potency for the OT-I TCR allow manipulation of the strength of TCR stimulation (Daniels et al., 2006; Hogquist et al., 1994; Hong et al., 2018; Rosette et al., 2001). In this study, we used the high potency SIINFEKL (N4), intermediate potency SIITFEKL (T4), and low potency SIIGFEKL (G4) peptides, as well as an unrelated control peptide, ASNENMDAM (NP68).

We designed a custom mass cytometry antibody panel to detect five surface markers of T cell identity and activation, eight phosphorylated signalling proteins with corresponding total proteins, and IκBα, which is degraded in response to stimulation (Figure 1; Methods). The antibodies labelled key components of major signalling pathways, including proximal signalling (pZAP70[Y319]/pSyk[Y352], pSLP76[Y128], pLCK[Y505] and pPLCγ1[Y783]), the

MAPK pathway (pERK1/2[T202/Y204]), the PDK1-PI3K and mTOR pathways (pAKT[S473], pS6[S235/S236]), the NFκB pathway (IκBα) and the IL2 pathway (pSTAT5[Y694]). All of these phosphorylation sites indicate active signalling with the exception of the inhibitory Y505 phosphorylation of LCK (D'Oro & Ashwell, 1999; Marth et al., 1988). Measurement of total proteins allowed us to determine whether changes in phospho-protein staining were due to differences in signalling or protein expression levels.

We isolated naïve $CD8^+$ T cells from OT-I *Rag1*$^{-/-}$ splenocytes before stimulating with ligands of various strengths. To monitor signalling while naïve $CD8^+$ T cells transitioned to activated T cells, and to relate signalling to changes in mRNA and protein expression during this process, cells were stimulated for 1, 2, 4 and 6 hours. We used a minimal, controlled system of peptide addition, allowing T cells to present antigens to each other. We also added exogenous IL2 to mitigate effects of potency-dependent differences in paracrine IL2 (Au-Yeung et al., 2017; Denton et al., 2011; Marchingo et al., 2014; Tan et al., 2017; Verdeil et al., 2006; Guillaume Voisinne et al., 2015) and provide all cells with an effector-promoting environment (Pipkin et al., 2010; Verdeil et al., 2006). This system was chosen in order to examine the cell-intrinsic effects of TCR stimulation strength on signalling pathways. Peptides were added at 1 μM since peptide titration revealed minimal differences in the percentage of cells phosphorylating S6 and ERK between 100 nM and 1 μM stimulation conditions (Figure 2- figure supplement 1). Using this reductionist stimulation system, we previously found that stimulation strength determined the rate with which naïve T cells initiated transcriptional activation but that cells activated by all ovalbumin-derived ligands were proliferating and expressing the effector molecule CD44 by two days (Richard et al., 2018).

Stimulated cells were stained with metal-conjugated antibodies and markers for dead cells and DNA before profiling by mass cytometry. We gated events detected by the mass cytometer in a hierarchical manner to select single, living cells that were TCRβ^+ and CD8α^+ before examining individual signalling molecules (Figure 2a). While gating for single cells based on DNA content (Figure 2 – figure supplement 2a), we noted that a substantial percentage of events contained more than one cell-equivalent of DNA, particularly among cells stimulated with the strongest peptide, N4 (Figure 2 – figure supplement 2b). Separating events by DNA content revealed two distinct populations, such that events containing two cell-equivalents of DNA had higher phosphorylated and total protein staining (Figure 2b, Figure 2 - figure supplement 2c-d). It is therefore likely that this population contained multiple cells (i.e. doublets), potentially even cells engaged in TCR-peptide-MHC interactions with their neighbours. After normalization of each phosphorylated protein to the DNA signal detected in the same mass cytometry event, signal intensities for events with two cell-equivalents of DNA had similar ranges to those of events with one for most markers (Figure 2 – figure supplement 2e). This provided further evidence that events with two cell-equivalents of DNA were doublets. Supporting the hypothesis that these doublets represented actively conjugated cells, a greater proportion of doublets than singlets showed signalling behaviour. In addition, from 1 to 4 hours after stimulation, pSLP76 signal was higher in doublet events even after normalisation, suggesting that SLP76 was preferentially phosphorylated in cells actively engaged in TCR-peptide-MHC interactions. Because it was not possible to discern which proteins were signalling in which cell in a multiplet event, for subsequent analyses we included only singlet events.

Ligand potency affects the kinetics of signalling protein activation

We next examined the kinetics of individual signalling molecules within our mass cytometry data. Total levels of signalling proteins did not substantially change over a 6 hour stimulation, while expression of effector proteins CD44 and CD25 increased in a time- and potency-dependent manner (Figure 3 – figure supplement 1). In the presence of exogenous IL2, ligand potency did not strongly influence the rate with which individual cells phosphorylated STAT5 (Figure 3 – figure supplement 2a). In the absence of exogenous IL2, STAT5 phosphorylation was associated with ligand potency, such that weak G4-stimulated cells showed no STAT5 phosphorylation (Figure 3 – figure supplement 2b), likely due to autocrine/paracrine IL2 rapidly secreted by strongly stimulated cells (Tan et al., 2017). The percentages of cells degrading IκBα or phosphorylating S6 or ERK1/2 were not impacted by the presence of exogenous IL2. The percentages of cells phosphorylating pAKT[S473] were subtly increased by IL2 particularly under stimulation with low potency ligands (Figure 3 – figure supplement 2b). This may reflect the mechanism proposed by Ross *et al* whereby JAK signalling induced by IL2 ultimately stimulates mTORC2 phosphorylation of AKT[S473] (Ross et al., 2016). Together, these data indicate the selectivity of IL2 effects on T cell signalling pathways.

Phosphorylation of proximal, membrane-recruited mediators ZAP70 and PLCγ1 was only detectable in a small percentage of cells at any point during this time course, preventing further interpretation (Figure 2b). For LCK, the percentage of cells with inhibitory phosphorylation of pY505 decreased at 6 hours in a potency-dependent manner, suggesting that stronger stimuli resulted in greater LCK activity only at this late time point (Figure 3 –

194 figure supplement 2a). For SLP76, the high potency ligand N4 induced a greater percentage
195 of signalling cells and greater signalling intensity within these cells between 1 and 4 hours,
196 whereas signalling was minimal in cells stimulated with intermediate (T4) or low potency
197 (G4) ligands (Figure 2b, Figure 3 – figure supplement 2a).
198
199 Examination of the kinetics of individual distal signalling molecules revealed two distinct
200 patterns. We defined these as transient if the percentage of signalling cells increased and
201 subsequently decreased during the time course of high potency stimulation, and sustained if
202 maximal signalling was ongoing at 6 hours (Figure 3a). ERK1/2, AKT and IκBα displayed
203 transient signalling. While ERK1/2 and AKT are phosphorylated in response to TCR
204 stimulation, IκBα is degraded, releasing NFκB subunits and permitting their translocation to
205 the nucleus (Paul & Schaefer, 2013). Therefore, a reduction in IκBα^{+} cells indicates active
206 signalling by this node. For these three signalling mediators, the percentage of cells actively
207 signalling was maximal at 2 hours when stimulated with the highest potency N4 peptide but
208 was delayed until 4 or 6 hours when stimulated with the lower potency T4 or G4 peptides
209 (Figure 3a). After 2 hours, signalling via these proteins declined in strongly stimulated cells,
210 resulting in a convergence with more weakly stimulated cells. In addition, the maximum
211 percentage of cells signalling through these nodes was substantially higher in strongly
212 stimulated cells. This may indicate repeated node activation after high potency stimulation,
213 such that a greater proportion of cells were signalling at any given time of measurement.
214 Thus, for these transiently signalling proteins, ligand potency was associated with the
215 maximal proportion of signalling cells and the speed with which this proportion was reached
216 on a populational level.
217

In contrast to these transient signalling events, S6 phosphorylation induced by TCR stimulation was sustained within our time course (Figure 3a). Under N4 stimulation, there was a rapid initial increase in the percentage of $pS6^+$ cells before a plateau. This pattern may be indicative of the signalling protein approaching saturation. The appearance of $pS6^+$ cells was slower after stimulation with lower potency ligands, but the proportions of $pS6^+$ cells approached convergence between N4, T4 and G4 stimulations at 6 hours. Thus, for S6, the rate with which cells exhibited active signalling, but not the maximal proportion of signalling cells was associated with ligand potency.

We observed a bimodal distribution of pERK1/2 measurements in our mass cytometry data, consistent with previous reports (Altan-Bonnet & Germain, 2005; J. Das et al., 2009; Tian et al., 2007). The extent of ERK1/2 phosphorylation in $pERK1/2^+$ cells, as determined by the median marker intensity, was unaffected by ligand potency (Figure 3 – figure supplement 3a). This confirmed that ERK1/2 exhibits digital signalling behaviour, *i.e.* on a per cell basis there is either an 'on' or 'off' state. Similarly, pS6[S235/S236] signal was also bimodally distributed (Figure 2a, Figure 3 – figure supplement 3b). The intensity of pS6 signal in $pS6^+$ cells slightly increased over time. Normalization to total S6 protein intensity mitigated this effect (particularly under strong stimulation) and suggested that ligand potency may subtly affect the rate of S6 phosphorylation within individual cells (Figure 3 – figure supplement 3c) in addition to the percentage of $pS6^+$ cells at early time points.

Since S6 phosphorylation at S235/S236 is driven by both S6K1 downstream of mTORC1, and RSK downstream of MEK1/2-ERK1/2 (Pende et al., 2004; Roux et al., 2007; R. J. Salmond et al., 2009), we were interested in how each of these pathways contributed to its digital

behaviour in strongly stimulated cells. To this end, we treated cells with inhibitors of MEK1/2 (MEK162 (Lee et al., 2010), Figure 3 – figure supplement 3d) and mTOR (rapamycin (Pollizzi & Powell, 2015)) before stimulation with N4 peptides. The per-cell phosphorylation of S6 decreased moderately in response to rapamycin (Figure 3b-c), with little difference between doses of 20 nM and 2 μM (Figure 3 – figure supplement 3e), but the bimodal distribution of pS6 and the percentage of $pS6^{+}$ cells were not disturbed. In contrast, while S6 phosphorylation also decreased within each cell in response to MEK162, this response was dose-dependent between 0.5 and 5 μM, and at the highest dose (5 μM), the bimodality was disturbed. In addition, even low doses of MEK162 halved the percentage of cells with phosphorylated S6 (Figure 3d). Combined MEK162 and rapamycin resulted in severe inhibition of S6 phosphorylation (Figure 3b). Neither MEK162, rapamycin, nor the combination of these two substantially impacted CD44 expression at the concentrations of inhibitors used (Figure 3 – figure supplement 3f), but a synergistic inhibition of cellular proliferation was observed after 2 days (Figure 3 – figure supplement 3g). Thus, simultaneous activity of the MEK and mTOR pathways is required for phosphorylating S6[S235/S236] and proliferative responses, and MEK signalling is essential for S6 digital phosphorylation. These data emphasize the coordinated nature of signalling downstream of the TCR.

Ligand potency determines the abundance of signalling cells but not the coordination of signalling events

To take advantage of the simultaneous measurements in mass cytometry data, we next tested for differential abundance of multidimensional cellular phenotypes, taking into

account all of the signalling markers measured (A. T. L. Lun et al., 2017) (Figure 4a, Figure 4 - figure supplement 1). We first defined 1585 fine-grained phenotypic states in the high dimensional space. We then compared the abundance of cells within these phenotypic states between unstimulated and all stimulated conditions (Methods). Clustering of significantly differentially abundant states revealed two main signalling phenotypes. Phenotype A, defined as $pS6^{+}$ $pSTAT5^{+}$ $pERK1/2^{+}$, was most prevalent in the high potency (N4)-stimulated cells. Phenotype B, defined as $pS6^{+}$ $pSTAT5^{+}$ $pERK1/2^{-}$, appeared under all stimulation conditions with uniform prevalence (Figure 4a). Phenotypes A and B were paralleled by the $pSTAT5^{-}$ phenotypes A' and B', respectively. Phenotypes A and A' were transient, whereas phenotypes B and B' were sustained. Subpopulation analysis confirmed that the high potency ligand N4 was capable of inducing a greater abundance of phenotypes A' ($pS6^{+}$ $pSTAT5^{-}$ $pERK1/2^{+}$) and A ($pS6^{+}$ $pSTAT5^{+}$ $pERK1/2^{+}$) up to 4 hours after stimulation (Figure 4b). In contrast, abundances of phenotypes B ($pS6^{+}$ $pSTAT5^{+}$ $pERK1/2^{-}$) and B' ($pS6^{+}$ $pSTAT5^{-}$ $pERK1/2^{-}$) increased at a similar rate between 1 and 6 hours after stimulation with all ovalbumin-derived ligands and were not associated with ordered ligand potency.

To complement these signalling phenotypes, we further investigated their relationship with surface expression of the effector protein CD44, which was an important contributor to phenotypic cluster separation (Figure 4a). We examined the 16 (2^4) possible states defined by combinations of the markers CD44, pS6, pSTAT5 and pERK1/2. The strongest peptide, N4, was capable of inducing a large proportion of $CD44^{-}$ $pS6^{+}$ $pSTAT5^{-}$ $pERK^{+}$ cells after 1 hour of stimulation (Figure 4c, Figure 4 - figure supplement 2). This was accompanied by an increasing population of $CD44^{-}$ $pS6^{+}$ $pSTAT5^{+}$ $pERK^{+}$ cells, which reached its maximum abundance 2 hours after stimulation. Cells stimulated by the weaker peptides T4 and G4

showed dramatically reduced abundances of these cellular phenotypes, and their maxima were delayed. For all stimuli, a high abundance of $CD44^-$ $pS6^+$ $pSTAT5^{+/-}$ $pERK1/2^-$ cells was seen between 4 and 6 hours. Cells expressed CD44 by 4 hours after strong and intermediate stimulation (N4 and T4) and by 6 hours after weak stimulation (G4).

From these data, we inferred the coordination of distal TCR-induced signalling. We propose that within our stimulation system, activating cells initially phosphorylate S6 and ERK1/2, followed by STAT5, after which ERK1/2 becomes dephosphorylated, followed by STAT5 in some cells. In the early hours after stimulation, signalling cells express CD44 at the same level as unstimulated cells but begin upregulating CD44 expression by 4-6 hours. As time progresses and cells shift to sustained phenotypes, those activated with reduced potency stimuli begin to phenotypically resemble those stimulated with high potency ligand (Figure 5). To formally test this order of activation events, we constructed activation trajectories of cells under each stimulation condition across all time points, based on their expression of pS6 (Figure 5 – figure supplement 1a). We then asked in what order along these trajectories pS6, pERK1/2, pSTAT5, and CD44 activation events were initiated (Figure 5 – figure supplement 1b-c). We found that pS6 appeared first, followed by pERK1/2, pSTAT5, and finally CD44. Of note, the start of ERK1/2 phosphorylation corresponded to the most dramatic increase in S6 phosphorylation, supporting evidence that ERK activation drives full S6[S235/S236] phosphorylation (Figure 3). The order of activation events was shared across stimulation conditions ($p = 0.00174$ compared to random orders of events, Methods). The signalling molecules pAKT, pLCK and IκBα were less dynamic along the trajectory, precluding precise determination of their order of activation particularly in weakly

stimulated cells, but visualizing their changes along the trajectory further suggested shared patterns between stimuli (Figure 5 – figure supplement 1d).

We therefore conclude that ligand potency controls the rate with which cells achieve certain signalling states and that the order of these signalling events is preserved regardless of stimulation strength.

Biosynthetic pathways are coordinately regulated downstream of TCR activation

Finally, we shifted our focus further downstream to examine the relationship between signalling at the ribosomal protein S6 and mRNA expression of early response transcription factors. These two activation events indicate initiation of translational and transcriptional processes, which are required for the biosynthetic programs of T cell activation (Araki et al., 2017; Howden et al., 2019; Tan et al., 2017). S6 is a ribosomal protein whose phosphorylation reflects, though it does not regulate, TCR-induced translation (R. J. Salmond et al., 2015; R. J. Salmond et al., 2009). *Nr4a1* (Nur77) and *Irf8* encode transcription factors that are rapidly expressed upon T cell activation (Moran et al., 2011; Nelson et al., 1996), and we previously found that their transcripts are upregulated at 1 and 3 hours, respectively, after strong N4 stimulation (Richard et al., 2018) (Figure 6 – figure supplement 1a). To examine these translational and transcriptional characteristics simultaneously, we activated naïve OT-I $CD8^+$ T cells with ligands of various potencies before measurement of pS6 and mRNA molecules using combined phosphoflow and RNA flow cytometry (Figure 6a, Figure 6 - figure supplement 1b).

Stimulation time courses with the different potency ligands suggested that *Nr4a1* transcripts were upregulated before phosphorylation of S6 and downregulated after, while *Irf8* transcripts were upregulated after S6 phosphorylation (Figure 6b, Figure 6 - figure supplement 1c). This order of events appeared consistent across stimuli. The percentage of $pS6^{+}$*Nr4a1*$^{+}$ cells was maximal between 1 and 2 hours after stimulation with the highest potency peptide N4, after 4 hours stimulation with the intermediate potency peptide T4, and after 6 hours stimulation with the lowest potency peptide G4. Likewise, the percentage of $pS6^{+}$*Irf8*$^{+}$ cells was maximal after 2 hours stimulation with N4, 4 hours stimulation with T4 and 6 hours stimulation with G4 peptides (Figure 6b). Similar to the multi-dimensional signalling phenotypes we measured by mass cytometry, these altered kinetics of phosphorylation and transcript upregulation indicate that stimulation strength controls their rate of activation.

These results suggest that the relationship between signalling events is conserved under different strengths of stimulation, even among differing signal transduction pathways controlling transcription and translation. Upon TCR activation both the transcriptional and translational machinery are deployed in a coordinated manner, which may improve efficiency of protein production enabling the naïve $CD8^{+}$ T cell to differentiate and proliferate.

Ligand potency affects the kinetics of selected signalling proteins in the presence of professional antigen-presenting cells

The interaction of adhesion molecules LFA-1 and ICAM-1 assists the formation of a stable immunological synapse, augments TCR-induced signalling, and continues to promote differentiation even after initial activation (Gérard et al., 2013; Verma & Kelleher, 2017). LFA-1 is constitutively expressed by naïve T cells, and TCR stimulation drives both redistribution and conformational changes that enhance its binding to the ligand ICAM-1 (Capece et al., 2017; Dustin & Springer, 1989; Verma & Kelleher, 2017). Palmer *et al* previously demonstrated that LFA-1-ICAM-1 interactions improve conjugate formation during T cell stimulation with peptide-loaded splenocytes, particularly for low potency ligands (Palmer et al., 2016). However, it remained unclear whether ICAM-1 was expressed in our stimulation system and whether this integrin interaction could thereby play a role. We therefore measured ICAM-1 on the surface of T cells 6 hours after addition of pure peptides of various potencies (Figure 7 – figure supplement 1a) and found that all T cells expressed ICAM-1, regardless of their stimulation status. These data suggest that integrin adhesion likely contributes to T cell activation along with TCR stimulation and exogenous IL2 in our system.

In contrast to this reductionist system, many additional factors impact T cell activation *in vivo*. Most fundamentally, naïve T cells are activated in the lymph node by professional antigen-presenting cells (APCs), such as dendritic cells, instead of other T cells. These APCs express costimulatory ligands in addition to peptide-MHC complexes, which can further tune naïve T cell responses (L. Chen & Flies, 2013; Hubo et al., 2013). For example, in our stimulation system, the costimulatory ligand CD80 remained largely absent after 6 hours of stimulation (Figure 7 – figure supplement 1a). In contrast, mature bone marrow-derived dendritic cells (BMDCs) expressed high levels of CD80, along with additional costimulatory

molecules (Figure 7 – figure supplement 1b). To test how signalling responses to ligands of different strengths might be impacted by the additional signalling conferred by professional APCs, we stimulated naïve T cells with mature BMDCs (Figure 7 – figure supplement 1b-c) loaded with peptides of various potencies. Exogenous IL2 was included to maintain comparability with the T:T stimulation system. Signalling molecules pZAP70, pSLP76, pERK1/2, pS6 and pSTAT5, as well as CD44 expression, were measured by flow cytometry.

We found that activation was in general less strong in the presence of peptide-pulsed professional APCs than pure peptides (Figure 7), perhaps due to reduced ligand availability as only half of the cells in the culture carried ligand (Methods). The potency-dependent kinetics of pERK1/2, pSLP67 and CD44 resembled those observed in the T:T stimulation system, while pZAP70 remained undetectable. pS6 was upregulated over time under stimulation with high, medium and low potency ligands. pSTAT5 was upregulated over time with all stimuli, including the null peptide NP68, suggesting that simply mixing naïve T cells with BMDCs enhanced IL2 signalling. These results indicate that the rate-based mechanism we observed in the T:T stimulation system is further tuned at particular signalling nodes by more complex antigen presentation.

Discussion

In this study, we examined the coordination of signalling pathways downstream of TCR activation using a custom mass cytometry panel as well as protein and RNA flow cytometry. The use of multidimensional measurements allowed us to probe the simultaneous activation of multiple signalling and transcriptional processes. This enabled comparisons of

the impact of ligand potency on not only individual activation events but also their coordination. We found that the strength of TCR stimulation controlled the rate of appearance of the multi-dimensional signalling and transcriptional phenotypes that we profiled.

Stimulation strength altering the rate of T cell activation has been observed in previous studies from our group and others investigating transcriptomic, proliferation, and protein expression characteristics (Hommel & Hodgkin, 2007; Richard et al., 2018; Rosette et al., 2001). Taken together, these data suggest that by controlling the probability that a cell will initiate activation responses, signal strength can modulate the average speed and magnitude of a population response. Our signalling results indicate that if such an activation switch exists, it lies very proximal to the TCR.

An important outstanding question is the mechanism by which the TCR translates ligand strength into the probability of downstream signalling. One model explaining the threshold for T cell response that could propagate to a rate-based mechanism is kinetic proofreading (McKeithan, 1995). This theory postulates that the ligand must remain bound to the receptor for sufficient time for signalling accumulation to surpass a critical event and propagate downstream. Indeed, multiple reports have suggested that naïve T cells require sustained interaction with presented antigen to achieve optimal proliferation, though the necessary duration differs by study and likely depends on the presence of additional factors such as IL2 (Renu Balyan et al., 2017; Curtsinger et al., 2003; Iezzi et al., 1998; Kaech & Ahmed, 2001; Prlic et al., 2006; van Stipdonk et al., 2003; van Stipdonk et al., 2001; Wong & Pamer, 2001). Refinements to the kinetic proofreading model suggest that not a single

interaction but rather the cumulative interaction lifetime of a series of early binding events controls signal accumulation (Dushek et al., 2009; Liu et al., 2014). Biophysical investigations of the impact of force on binding events between the TCR and pMHC (as well as CD8) have described catch bonds formed with high potency ligands that extend interaction lifetimes (D. K. Das et al., 2015; Hong et al., 2018; Liu et al., 2014; Sibener et al., 2018; P. Wu et al., 2019), though this observation has not been universal (Limozin et al., 2019) and merits further investigation. Extrapolating from this lifetime theory, altered ligand potency could change the probability of long or rapidly repeated binding events, thereby controlling the probability that an individual cell activates.

If such a lifetime-based mechanism exists, T cells must then translate variation in binding lifetime to the presence or absence of downstream signalling. Palmer and colleagues found ligand potency-associated differences in CD3ζ chain and ZAP70 phosphorylation (Daniels et al., 2006; Palmer et al., 2016), which may allow potency-dependent accumulation of signal before propagation downstream. Supporting this hypothesis, John James demonstrated that the number of CD3 ITAM motifs in a synthetic receptor influenced the rate but not the magnitude of signalling within individual Jurkat cells (James, 2018). Likewise, Mukhopadhyay *et al.* found that the presence of multiple ζ chain ITAMs, as well as ZAP70, increases the efficiency of phosphorylation in a HEK 293T cell reconstitution system, although these phosphorylation events do not account for the apparent switch-like ultrasensitive behaviour of T cell signalling (Mukhopadhyay et al., 2016). One mechanism that could explain the switch-like behaviour is the zero-order ultrasensitivity model (Ferrell & Ha, 2014; Goldbeter & Koshland, 1981), wherein negative regulators act in combination with activators to enhance responsiveness when signalling molecules operate close to

456 saturation. In this way, a relatively small change in the binding lifetime of a pMHC ligand
457 could be amplified by altering a kinase/phosphatase ratio to switch between the presence
458 and absence of downstream signalling. An alteration in the local relative abundances of
459 phosphatase CD45 and kinase LCK described by the kinetic segregation model (Davis & van
460 der Merwe, 2006; Razvag et al., 2018) represents an intriguing candidate for controlling a
461 zero-order ultrasensitivity mechanism (Hui & Vale, 2014), although a subsequent study has
462 refuted its requirement for T cell activation (Al-Aghbar et al., 2018), suggesting other
463 mechanisms. Control may also be mediated by the phosphatase PTPN22, which can
464 dephosphorylate CD3ζ chains, ZAP70 and LCK (J. Wu et al., 2006), as absence of PTPN22
465 results in increased proportions of activated cells, particularly under weak stimulation
466 (Robert J Salmond et al., 2014). Alternatively, Lo *et al.* showed that the slow
467 phosphorylation of a tyrosine residue in LAT is a possible candidate for this rate-limiting
468 step, since substitution of a single residue that enhances this phosphorylation improves T
469 cell response to low potency ligands (Lo et al., 2019).
470
471 Through our single-cell measurements, we confirmed (Altan-Bonnet & Germain, 2005; J. Das
472 et al., 2009; Tian et al., 2007) that ERK1/2 is phosphorylated with 'on or off' states,
473 characteristic of digital signalling. In addition, we found that S6[S235/S236] is also
474 phosphorylated in a similar manner. However, whilst the extent of ERK1/2 phosphorylation
475 during the "on" state was constant, the extent of S6 phosphorylation subtly increased both
476 with time and strength of stimulus. The parallel subtle increase in total S6 expression over
477 time implies induction of S6 protein production during T cell activation. These data suggest
478 that dividing signalling proteins into digital or analogue can be complicated by changes in
479 total protein levels that may attribute analogue properties to a digital signal.

Previous work has shown that in addition to mTORC1 signalling, the MEK/ERK pathway contributes to S6[S235/S236] phosphorylation (Pende et al., 2004; Roux et al., 2007), particularly in naïve T cells (Krishnaswamy et al., 2014). Therefore, combinatorial effects of mTORC1 and MEK signalling might be expected to influence both S6 phosphorylation and other downstream T cell activation phenotypes. We found that chemical inhibition of both of these pathways blocked S6 phosphorylation, implying that they contribute in a non-redundant manner. A dose titration with MEK162 indicated that MEK/ERK signalling is critical for phosphorylation of S6[S235/S236]. Even at low doses, MEK162 reduced the percentage of $pS6^{+}$ cells, suggesting that it may modulate the rate of response. Furthermore, in our trajectory analysis of multiple signalling markers, a steep increase in S6 phosphorylation coincided with the appearance of $pERK^{+}$ cells under all peptide stimuli (Figure 5 – figure supplement 1a-b). These data raise the possibility that digital phosphorylation of ERK propagates through RSK to S6[S235/S236].

We additionally explored the effects of rapamycin and MEK162 on naïve T cell proliferation. Although rapamycin had little effect on S6 phosphorylation, it had a profound effect on T cell proliferation, which may be due to several different mechanisms. First, rapamycin can also impact mTORC2 signalling after prolonged treatment (Sarbassov et al., 2006), and naïve T cells may be particularly susceptible (Delgoffe et al., 2011). Second, mTORC1 affects many additional pathways other than ribosomal activity (Pollizzi & Powell, 2015; R. J. Salmond, 2018). Finally, even when signalling through S6K1, mTORC1 can influence proliferation through pS6-independent mechanisms (R. J. Salmond et al., 2015). We also found that MEK

503 inhibition with MEK162 synergized with rapamycin to further dampen T cell proliferation,
504 highlighting the interconnected nature of the signalling pathways downstream of the TCR.
505
506 Many signalling molecules exhibited transient behaviour at the population level (ERK1/2,
507 IκBα, AKT), while pS6 accumulated over the course of our 6-hour experiments. Stimulation
508 strength strongly influenced the proportion of cells exhibiting transient signalling behaviours
509 between 1 and 4 hours after activation, but by 6 hours, cells activated with any of the
510 ovalbumin-derived peptide ligands exhibited a similar signalling phenotype. This potency-
511 dependent difference in the maximal proportions of cells signalling may be due to either
512 repeat or sustained signalling with strong ligands, the latter of which has been observed for
513 calcium fluxes induced by TCR stimulation (J. L. Chen et al., 2010; Le Borgne et al., 2016;
514 Wulfing et al., 1997). For example, although under weak G4 stimulation only a very small
515 percentage (15.4%) of cells were found to be pERK1/2^{+} at any given time, the majority
516 (72.1%) of G4-stimulated cells achieved digital activation of pS6[S235/236] by 6 hours
517 (Figure 3a). Given that we found full S6 phosphorylation after strong stimulation requires
518 MEK signalling, we hypothesize that this pathway is active in all stimulation conditions but
519 that ERK activation events occur with reduced frequency or duration with weak stimuli and
520 thus many were missed in our snapshot measurements. Future investigations using ERK
521 reporters and ERK inhibition in weakly stimulated cells would be needed to test this
522 prediction. Consistent with this proposed mechanism, single-cell studies in epithelial and
523 HEK293 cell lines have observed oscillating ERK phosphorylation with frequency and
524 duration dependent on the concentration or frequency of EGF stimulation (Albeck et al.,
525 2013; Ryu et al., 2018). Such an effect on digital ERK activation may be modulated by multi-
526 step activation of the upstream mediator SOS dependent on its dwell-time after activation-

induced recruitment to the plasma membrane (Huang et al., 2019). Interestingly, using a light-inducible ERK activation system in epithelial cells, Aoki *et al* demonstrated divergent transcriptional effects of sustained versus transient ERK activation (Aoki et al., 2013). It therefore remains possible that different ERK targets in T cells, such as translational machinery, microtubule remodelling, and transcription factors (e.g. ELK1, SAP1, SAP2) (Navarro & Cantrell, 2014) are differentially affected by stimulation strength, warranting further investigation of additional downstream components.

Examination of the coordinated activation of transcriptional and translational signalling pathways also revealed conservation of this order of events. Biosynthetic processes are critical for naïve T cells to differentiate into effector cells (Araki et al., 2017; Tan et al., 2017), and thus, carefully controlled simultaneous activation would ensure efficient, consistent effector differentiation of activated cells.

Under stimulation with peptide-loaded BMDCs, ligand potency determined the percentages of T cells undergoing certain activation events (pERK1/2, pSLP76 and CD44), similar to observations in our reductionist stimulation system. In contrast, phosphorylation of S6 was not associated with ligand potency after stimulation with peptide-loaded BMDCs. Unlike naïve and recently activated T cells, BMDCs express high levels of costimulatory molecules that can impact TCR-induced signalling. For example, ligation of the costimulatory receptor CD28 at the same time as the TCR results in amplification of signalling pathways including NFAT, NFκB and AP-1, and can enhance both the sensitivity and ultimate division potential of naïve T cell activation (Esensten et al., 2016; Heinzel et al., 2017; Marchingo et al., 2014; Yang et al., 2017). Further exploration of how individual costimulatory ligands impact the

coordination and initiation rate of the TCR-induced signalling programme will be important for dissecting these additional inputs.

Despite the increased complexity of BMDC peptide presentation, this *in vitro* system is nevertheless still far-removed from *in vivo* T cell activation, where the microenvironment is increasingly complex. Additional variables such as cytokine and nutrient availability and cell-cell interactions can further tune the T cell response *in vivo* (Curtsinger & Mescher, 2010; Kedia-Mehta & Finlay, 2019). Moreover, strongly stimulated T cells undergo prolonged retention in the lymph node (Ozga et al., 2016; Zehn et al., 2009) and may out-compete weakly stimulated T cells for cytokines and nutrients (Wensveen et al., 2012), suggesting that stimulation strength and the microenvironment are not independent. Our controlled *in vitro* systems allowed us to identify effects of stimulation strength on TCR-induced pathways alone, as well as in the context of BMDC-mediated costimulation, without confounding by other *in vivo* factors and feedback. By delineating the impact of stimulation strength in low-complexity systems, these data can form the basis for interpretation of future studies where additional variables may be explored.

In this study, we measured 22 markers of protein expression and active signalling. While other unmeasured signalling mediators may respond to altered stimulation strength in a different manner, our data demonstrate a strict choreography of the distal signalling processes that we examined. Stimulation strength was associated with the rate with which cells embarked on this regimented programme. This suggests that using a limited set of signalling machinery in a single coordinated programme, T cells can finely tune their responses to different ligands through modulation of the rate of signalling.

Methods

Key Resources

Key resources are detailed in Supplementary File 2.

Ethics

Animal experimentation: Experiments were carried out under Project Licence PPL 70/8590. This research has been regulated under the Animals (Scientific Procedures) Act 1986 Amendment Regulations 2012 following ethical review by the University of Cambridge Animal Welfare and Ethical Review Body (AWERB).

Mice

$CD8^+$ T cells were isolated from OT-I *Rag1*-deficient mice (OT-I *Rag1*^{tm1Bal} on a C57BL/6 background), which underwent confirmation of genotype prior to study. BMDCs were generated from wild-type C57BL/6 mice. Experiments used both male and female mice 9-25 weeks old. Mice were bred and maintained within University of Cambridge animal facilities.

Cell culture and stimulation

For T cell isolation, single cell suspensions of splenocytes were produced via homogenization of the spleen through a 70 µM nylon strainer. $CD8^+$ T cells were isolated

using the Mouse CD8α^+ T cell Isolation Kit (MACS Miltenyi Biotec). Cells were cultured in RPMI 1640 (Gibco), 10% FBS (Biosera), penicillin-streptomycin (Sigma), sodium pyruvate (Gibco), L-glutamine (Sigma), β-mercaptoethanol (Gibco) and 20 ng/ml recombinant mouse IL-2 (Peprotech). For stimulation, the following peptides were used at the concentrations indicated: SIINFEKL (N4), SIITFEKL (T4), SIIGFEKL (G4), and ASNENMDAM (NP68) (Cambridge Bioscience).

Bone marrow derived dendritic cells (BMDCs) were generated based on a published protocol by Abcam. Femurs and tibias were sterilized in 70 % ethanol and flushed with cold BMDC culture media, consisting of RPMI 1640 (Gibco), 10 % FBS (Biosera), penicillin-streptomycin (Sigma), L-glutamine (Sigma) and β-mercaptoethanol (Gibco). The suspension of bone marrow progenitor cells was passed through a 70 µM nylon strainer and plated in 10 cm petri dishes in BMDC culture media supplemented with 20 ng/ml GM-CSF (Peprotech). Fresh BMDC culture media with 20 ng/ml GM-CSF was added on day 3 and replaced on day 6 and, if needed, day 8. Immature dendritic cells were harvested from day 7 to day 9. Maturation was induced by culturing immature dendritic cells for 1 day in BMDC culture media with 20 ng/ml GM-CSF, as well as 50 ng/ml LPS (Thermofisher Scientific) and 20 ng/ml IL4 (Abcam). Differentiation into immature and mature BMDCs was verified by flow cytometry. To stimulate T cells, mature BMDCs were pulsed with 1 µM of peptide for 1 hour at 37 °C, washed, mixed with naïve T cells at a ratio of 1:1, and cultured for the times indicated.

Mass cytometry

623 Purified naïve $CD8^+$ T cells were analysed by mass cytometry. In experiment 1, cells from 4
624 age-matched mice (2 males and 2 females) were used, representing 4 biological replicates.
625 In experiment 2, more stimulation conditions were included. This necessitated more cells
626 for each biological replicate than could be obtained from a single mouse. Therefore, each
627 biological replicate (1 male, 1 female) was composed of cells from a pair of age- and gender-
628 matched mice. Staining for mass cytometry was performed using sequential MaxPar reagent
629 kits (Fluidigm) in the following steps. Live cells were stained with 5 µM Cell-ID Cisplatin for 5
630 minutes at 37°C and rested for 15-30 minutes before stimulation with 1 µM N4, T4, G4, or
631 NP68 peptides, or left unstimulated. In Experiment 1, cells were stimulated for 1 and 2
632 hours. In Experiment 2, cells were stimulated for 1, 2, 4 and 6 hours. See Supplementary File
633 1 for replicate structure. Cells were fixed with Maxpar Fix I Buffer for 10 minutes at room
634 temperature. Cells stimulated under different conditions were barcoded using the Cell-ID
635 20-Plex Pd Barcoding Kit and pooled for staining to minimise confounding technical
636 differences. In experiment 1, all cells from each mouse were pooled into a batch. In
637 experiment 2, in addition to pooling within a biological replicate, 4 samples were shared
638 across the two pools to enable batch normalization for differential abundance analysis as
639 described below. Cells were blocked with FCR blocking reagent (Biolegend, clone 93) and
640 stained with metal-conjugated surface antibodies (Supplementary File 3). Surface-stained
641 cells were permeabilised with methanol (Fisher Scientific) and stained with metal-
642 conjugated antibodies against intracellular targets (Supplementary File 3), all diluted in
643 Maxpar Cell Staining Buffer. Stained cells were then fixed with 1.6 % formaldehyde
644 (Thermofisher) and stained overnight with 125 nM Cell-ID Intercalator-Ir in Maxpar Fix and
645 Perm Buffer. Cells were analysed on a Helios CyTOF system (Fluidigm). Data within each cell
646 pool was normalized and debarcoded using the Fluidigm CyTOF software.

Mass cytometry antibodies

Metal-conjugated antibodies were custom-conjugated where not already commercially available (Supplementary File 3). All custom-conjugated antibody clones were tested using phosphoflow cytometry before and after metal-conjugation. When allocating metals to antibody targets, brighter metals were assigned to antibodies that exhibited weaker phosphoflow staining or to those without clear bimodal expression. Metal channels that receive significant cross-over from other channels were also allocated antibodies with stronger signals. For each protein target, antibodies against the total protein and its phosphorylated version were conjugated to metals differing by more than one mass unit to avoid spillover.

Antibodies targeting phosphorylated proteins were validated using phosphoflow (with and without metal conjugation) under different stimulating conditions, including anti-CD3 coated plate (1 μg/ml, BD Biosciences, clone 145-2C11), PMA (50 nM, Sigma-Aldrich) and ionomycin (1 μg/ml, Sigma-Aldrich), N4 peptide (1 μM), and pervanadate (1 mM, prepared using sodium orthovanadate, Sigma-Aldrich) (Supplementary File 4). To confirm the specificity of the antibody clones targeting ZAP70, LCK and SLP76, we transfected HEK 293T cells, which lack endogenous expression of these proteins, with vectors encoding the proteins and tested antibody binding via flow cytometry and immunofluorescence (Supplementary File 4a). To confirm the specificity of the antibody clone targeting PLCγ1 (3H1C10), we performed siRNA knockdown in T cells and tested antibody binding by flow cytometry (Supplementary File 4a). (Knockdown was validated by western blotting with a

WB-specific antibody clone (D9H10).) Further validation of phospho-specific antibodies was performed using signalling inhibitors as detailed in the antibody specificity tables (Supplementary File 4).

All metal-conjugated antibodies were tested by mass cytometry prior to experimentation. By testing antibodies on fixed cells, fixed and barcoded cells, and live cells (surface markers only), we confirmed there was no additional loss of antibody activity through the addition of the barcoding step. Two surface markers performed less well when fixed (CD62L-160Gd clone MEL-14 and CD69-143Nd clone H1.2F3, both Fluidigm). The CD62L-160Gd antibody was excluded from the mass cytometry panel. The CD69-143Nd antibody was excluded from the analyses in experiment 1, and excluded from the staining panel in experiment 2. All metal-conjugated antibodies were titrated for optimal performance and key signalling antibodies were tested in a time-course assay under different stimulatory conditions to determine the optimal times for running the full panel.

Mass cytometry data analysis

For mass cytometry analysis in FlowJo (v10), debarcoded samples were gated in a hierarchical manner: EQ bead exclusion followed by selection of intact cells based on DNA content, single cells based on the event length and DNA content, living cells based on cisplatin staining, and finally $CD8\alpha^+$ $TCR\beta^+$ cells. For activation-induced markers, positive/negative status was defined based on comparison with unstimulated cells.

Normalization of antibody-measured signals to DNA signal, as well as phospho-protein to total protein signals, was performed in R using the ncdfFlow (v2.30.1) (Gopalakrishnan, 2019) and flowCore (v1.50.0) (Hahne et al., 2009) Bioconductor packages. The signal of each marker in each event was normalized to the signal from the 191Ir DNA channel or appropriate total protein channel within that event. Normalized ratios were then scaled to the median 191Ir DNA or appropriate total protein signal from one selected sample for visualization purposes.

To test for differential abundances, mass cytometry data from experiment 2 was processed using the ncdfFlow (v2.30.1), flowCore (v.1.50.0) and cydar (v1.8.0) (A. T. L. Lun et al., 2017) Bioconductor Packages in R. A logicle transformation (default parameters except w=0.1) was applied to raw intensity data. Data from the two batches were range-normalized based on the 4 samples that were included in both batches using the normalizeBatch function (with parameters p=0.001, fix.zero=TRUE). After normalization, one technical replicate from each of these four repeated samples was carried forward for analysis. All samples were then pooled before constructing the sequential gating strategy: removal of residual EQ beads, removal of events with high event length, retaining events with a single cell-equivalent of DNA, removal of dead cells, removal of cells with TCRβ signal more than 5 MAD below the median, and removal of cells with CD8 signal more than 5 MAD below the median. Cells from each sample were down-sampled to the number in the smallest sample (10,982). Only signalling proteins and selected surface markers were included in differential abundance testing to avoid invariant and non-biological markers: pSTAT5, pAKT, pSLP76, pLCK, IκBα, pPLCγ1, pERK1/2, pZAP70, pS6, CD8α, CD44, CD25, TCRβ, CD45.

To test for differential abundance of cells with any combinatorial phenotype, agnostic to cellular density or clustering patterns, we employed cytometry differential abundance testing in R (cydar, (A. T. L. Lun et al., 2017)). This method takes advantage of the consistent staining achieved with sample barcoding, along with the count-based nature of single cell data, to find regions of the high-dimensional marker space occupied significantly more or less frequently by cells from a particular condition. This is achieved by filling the marker space with hyperspheres, comparing cellular abundances within each hypersphere across conditions, and controlling the false discovery rate across the marker space. Cells were assigned to hyperspheres and counted using the prepareCellData, neighborDistances, and countCells functions from cydar (default parameters except countCells tol=0.4 and downsample=200). Hyperspheres were included in differential abundance analysis if they contained more than 50 cells on average. Differential abundance was assessed using the edgeR (v3.26.8) Bioconductor package (A. T. Lun et al., 2016; Robinson et al., 2010) with a robust quasi-likelihood GLM fit (A. T. L. Lun et al., 2017) including the biological replicate of origin as a blocking factor for each sample in an analysis of deviance test to identify hyperspheres that changed in abundance in any stimulation condition compared to the unstimulated control. The spatial FDR was controlled at 0.05 to define significantly differentially abundant hyperspheres. See Supplementary File 5 for full summary statistics from differential abundance testing.

For trajectory analysis, each biological replicate was analysed separately. A logicle transformation (default parameters except w=0.1) was applied to raw intensity data. Cells within each replicate were then gated using the sequential strategy described above. The MAD threshold for TCRβ^+ cells was relaxed in gating biological replicates from experiment 1

due to a wider distribution in this dataset. To construct trajectories, equal numbers of cells stimulated by each ovalbumin-derived ligand were pooled with unstimulated cells. This created one sample per ligand (N4, T4 and G4) per biological replicate from which to construct trajectories. For each trajectory, cells were ordered by intensity of pS6 as this marker was observed to increase with activation over real time. Colouring cells by real time point confirmed enrichment of cells sampled at early times at the beginning of the trajectory and later times at the end (Figure 5 – figure supplement 1a). To generate plots in Figure 5 - figure supplements 1b-c, a loess curve was fitted to intensity measurements of the indicated markers across 2000 randomly sampled cells from each trajectory (span = 0.2). To determine the trajectory interval in which each activation event started, trajectories were downsampled to 5000 cells each, and a sliding window encompassing 5 % of the trajectory was established to move across the trajectory from least to most activated in steps of 1 %. The first window in which the mean intensity of cells was more than one standard deviation away from the mean intensity in the starting window was deemed the initiation of the activation event. Events that displayed a shift in mean intensity across the trajectory but fell short of the threshold (CD44 under G4 stimulation), were considered to be last in the ordering. If more than one activation event failed to meet this threshold in a given trajectory, or if two events shared an initiation window, it was not possible to robustly declare the order. The probability of achieving orders of signalling events shared to the observed extent or more between each pair of trajectories was then computed by comparing the mean-squared-distance (MSD) between the orders in trajectory 1 and trajectory 2 to a distribution of MSDs between the orders in trajectory 1 and permuted orderings of trajectory 2. Both biological replicates from experiment 2 that contained all time-points revealed identical orders of activation events across all stimulation conditions.

766 The two biological replicates in experiment 1 that included 0, 1 and 2 hours of stimulation
767 also revealed the same order of activation of pS6 and pERK, while pSTAT5 and CD44 were
768 not sufficiently activated by 2 hours to determine their ordering. It was not possible to order
769 events in the remaining biological replicates from experiment 1 that included only 1
770 stimulated timepoint.
771
772 **Flow cytometry**
773
774 To test BMDC maturation, cells were stained with live-dead marker (Zombie-NIR or Zombie-
775 Aqua Fixable Viability Kit, Biolegend) in PBS before staining in incubation buffer (1 % FBS in
776 PBS) with FCR (FC receptor) blocking antibody (Biolegend, clone 93) and antibodies against
777 CD11c, MHC II, CD80, CD86, CD40 and ICAM1 (Supplementary File 2). Cells were acquired on
778 a BD LSRFortessa. Data were analysed in FlowJo (v10) gating on single, live cells. BMDCs
779 were consistently > 90 % $CD11c^+$ and MHC II^+ (Figure 7 – figure supplement 1b). To measure
780 CD80 and ICAM-1 expression on activated T cells, T cells were stained with live-dead marker
781 (Zombie-NIR Fixable Viability Kit, Biolegend) and antibodies against CD80 and ICAM1 in the
782 same way.
783
784 To test the impact of inhibiting the MEK and mTOR pathways on cell proliferation (Figure 3 –
785 figure supplement 3g), cells were stained with eBioscience Cell Proliferation Dye eFluor-450
786 (ThermoFisher), pre-treated for 2 hours with MEK162 (1 µM and 5 µM), rapamycin (200 nM)
787 or combined MEK162 (1 µM or 5 µM) and rapamycin (200 nM), and stimulated with 1 µM
788 N4 or NP68 peptides for 2 days. Cells were then stained with live-dead marker (Zombie-NIR

Fixable Viability Kit, Biolegend) and acquired on a BD LSRFortessa and data analysed in FlowJo (v10) gating on live, single cells.

Phosphoflow cytometry

For phosphoflow cytometry experiments in Figure 2 - figure supplement 1, Figure 3b-d, Figure 3 - figure supplements 2 and 3, and Figure 7, after stimulation, cells were fixed in 4 % paraformaldehyde (Electron Microscopy Sciences) at room temperature for 15 minutes and washed in PBS. Cells were permeabilized with 90 % ice-cold methanol (Fisher Scientific) for 30 minutes on ice or overnight at -20 °C. Cells were washed in PBS and resuspended in 100 µL incubation buffer containing FCR blocking antibody (Biolegend, clone 93), stained with the primary antibodies of interest (Supplementary File 2), and incubated for 1 hour at room temperature. In cases where the primary antibody was not conjugated to a fluorophore, the cells were then washed, resuspended in 100 µL incubation buffer containing FCR blocking antibody and secondary antibody (Supplementary File 2) and incubated for 30 minutes at room temperature. Cells were washed in incubation buffer prior to data acquisition on a BD LSRFortessa. Data were analysed in FlowJo (v10) gating on single, live cells.

To test the impact of titrating peptides on the phosphorylation of ERK and S6 (Figure 2 – figure supplement 1), cells stained with live-dead marker (Zombie-NIR Fixable Viability Kit, Biolegend) were stimulated with N4, T4, G4 and NP68 peptides at concentrations of 10 nM, 100 nM and 1 µM for 2 and 4 hours.

To test the impact of adding or withholding exogenous IL2 on phosphorylation of STAT5, S6, ERK, and AKT, and degradation of IκBα (Figure 3 – figure supplement 2), cells stained with a live-dead marker (Zombie-NIR Fixable Viability Kit, Biolegend) were stimulated with 1 μM of peptides for 4 hours.

To test the impact of inhibiting the MEK/ERK and mTOR/S6 pathways (Figure 3b-d, figure supplement 3d-f), cells stained with live-dead marker (Zombie-NIR Fixable Viability Kit, Biolegend) were pre-treated with the MEK inhibitor MEK162 (binimetinib/ARRY-162/ARRY-438162, Selleckchem), mTOR inhibitor rapamycin (Sigma-Aldrich) or combined MEK162 and rapamycin for 2 hours. MEK162 was added at 0.5 μM, 1 μM and 5 μM, rapamycin was added at 20 nM, 200 nM and 2 μM. For combined drug treatments, MEK162 was added at 0.5 μM, 1 μM and 5 μM with rapamycin at 200 nM. DMSO as a vehicle control was added at 1:1000, corresponding to the amount in the 200 nM dose of rapamycin and the 1 μM dose of MEK162. Cells were stimulated with 1 μM of N4 or NP68 peptides for 4 hours.

To test naïve T cell stimulation with peptide-loaded BMDCs, T cells were stained with live-dead marker (Zombie-NIR Fixable Viability Kit, Biolegend) before co-culture with BMDCs.

Combined phosphoflow with RNA flow cytometry

To combine phosphoflow with RNA flow cytometry (Figure 6 and figure supplement 1b-c), purified naïve CD8α$^+$ T cells were stained using a live-dead marker (Zombie Aqua Fixable Viability Kit, Biolegend). To achieve a sufficient number of cells, isolated naïve CD8$^+$ T cells from three age- and gender-matched mice were pooled for each biological replicate. Cells

836 were stimulated for 0-6 hours with 1 µM N4, T4, G4, or NP68 peptides. At the end of
837 stimulation, cells were immediately moved on to ice and washed with cold PBS. Cells were
838 fixed and permeabilised using the Primeflow RNA Assay Kit (ThermoFisher Scientific),
839 blocked with FCR blocking reagent (Biolegend, clone 93) and stained with antibodies against
840 pS6[S235/236] (BD Biosciences clone N7-548) for 30 minutes. Cells were stained with the
841 following PrimeFlow probe sets (Thermofisher Scientific): *Nr4a1* AF647 (Type1, VB1-12484-
842 204), *Irf8* AF750 (Type 6, VB6-3197312-210), and *Rpl39* AF488 (Type 4, VB4-3120826-204) as
843 a control. The use of *Rpl39* as a control gene was previously described in naïve and recently
844 activated $CD8^+$ T cells (Richard et al., 2018). Cells were acquired on a BD LSRForessa and
845 analysed in FlowJo (v10). Cells were gated on single, live cells that expressed *Rpl39,* to
846 ensure cells were permeabilized and probes hybridized and amplified.
847

Code availability statement

Analysis code for mass cytometry data is available at:
https://github.com/MarioniLab/SignallingMassCytoStimStrength

Data availability statement

Mass cytometry data are available in the Flow Repository, accession numbers FR-FCM-Z2CX and FR-FCM-Z2CP.

Acknowledgements

This work was funded by the Wellcome Trust (grants [103930], [100140] and [217100] to G.M.G and grant 204017/Z/16/Z to C.Y.M); Cancer Research UK (core funding [A17197] to J.C.M); EMBL (core funding to J.C.M); the MRC (MR/P014178/1 to A.C.R); the ACT (grant [23/17 A (ii)] to C.Y.M). A.C.R also received a pump-priming grant from the National Institute for Health Research [Cambridge Biomedical Research Centre at the Cambridge University Hospitals NHS Foundation Trust]; the views expressed are those of the authors and not necessarily those of the NHS, the NIHR or the Department of Health and Social Care. This research was supported by the CIMR and CRUK-CI Flow Cytometry Core Facilities. We thank M. Strzelecki and R. Grenfell for their assistance and support in processing samples for mass cytometry, and A. Lun for his advice and support on analysing mass cytometry data.

872

873

874 **Competing interests**

875

876 The authors declare no competing interests.

References:

Al-Aghbar, M. A., Chu, Y.-S., Chen, B.-M., & Roffler, S. R. (2018). High-affinity ligands can trigger T cell receptor signaling without CD45 segregation. *Frontiers in immunology, 9*, 713.

Albeck, J. G., Mills, G. B., & Brugge, J. S. (2013). Frequency-modulated pulses of ERK activity transmit quantitative proliferation signals. *Mol Cell, 49*(2), 249-261. doi:10.1016/j.molcel.2012.11.002

Altan-Bonnet, G., & Germain, R. N. (2005). Modeling T cell antigen discrimination based on feedback control of digital ERK responses. *PLoS Biol, 3*(11), e356. doi:10.1371/journal.pbio.0030356

Aoki, K., Kumagai, Y., Sakurai, A., Komatsu, N., Fujita, Y., Shionyu, C., & Matsuda, M. (2013). Stochastic ERK activation induced by noise and cell-to-cell propagation regulates cell density-dependent proliferation. *Mol Cell, 52*(4), 529-540. doi:10.1016/j.molcel.2013.09.015

Araki, K., Morita, M., Bederman, A. G., Konieczny, B. T., Kissick, H. T., Sonenberg, N., & Ahmed, R. (2017). Translation is actively regulated during the differentiation of CD8(+) effector T cells. *Nat Immunol, 18*(9), 1046-1057. doi:10.1038/ni.3795

Au-Yeung, B. B., Smith, G. A., Mueller, J. L., Heyn, C. S., Jaszczak, R. G., Weiss, A., & Zikherman, J. (2017). IL-2 modulates the TCR signaling threshold for CD8 but not CD4 T cell proliferation on a single-cell level. *The Journal of Immunology, 198*(6), 2445-2456.

Balyan, R., Brzostek, J., & Gascoigne, N. R. J. (2018). CD8(+) T cells have commitment issues. *Nat Immunol, 19*(8), 797-799. doi:10.1038/s41590-018-0169-0

Balyan, R., Gund, R., Ebenezer, C., Khalsa, J. K., Verghese, D. A., Krishnamurthy, T., George, A., Bal, V., Rath, S., & Chaudhry, A. (2017). Modulation of naive CD8 T cell response features by ligand density, affinity, and continued signaling via internalized TCRs. *The Journal of Immunology, 198*(5), 1823-1837.

Bandura, D. R., Baranov, V. I., Ornatsky, O. I., Antonov, A., Kinach, R., Lou, X., Pavlov, S., Vorobiev, S., Dick, J. E., & Tanner, S. D. (2009). Mass cytometry: technique for real time single cell multitarget immunoassay based on inductively coupled plasma time-of-flight mass spectrometry. *Anal Chem, 81*(16), 6813-6822. doi:10.1021/ac901049w

Bendall, S. C., Simonds, E. F., Qiu, P., Amir el, A. D., Krutzik, P. O., Finck, R., Bruggner, R. V., Melamed, R., Trejo, A., Ornatsky, O. I., Balderas, R. S., Plevritis, S. K., Sachs, K., Pe'er, D., Tanner, S. D., & Nolan, G. P. (2011). Single-cell mass cytometry of differential immune and drug responses across a human hematopoietic continuum. *Science, 332*(6030), 687-696. doi:10.1126/science.1198704

Capece, T., Walling, B. L., Lim, K., Kim, K.-D., Bae, S., Chung, H.-L., Topham, D. J., & Kim, M. (2017). A novel intracellular pool of LFA-1 is critical for asymmetric CD8+ T cell activation and differentiation. *Journal of Cell Biology, 216*(11), 3817-3829.

Chen, J. L., Morgan, A. J., Stewart-Jones, G., Shepherd, D., Bossi, G., Wooldridge, L., Hutchinson, S. L., Sewell, A. K., Griffiths, G. M., van der Merwe, P. A., Jones, E. Y., Galione, A., & Cerundolo, V. (2010). Ca2+ release from the endoplasmic reticulum of NY-ESO-1-specific T cells is modulated by the affinity of TCR and by the use of the CD8 coreceptor. *J Immunol, 184*(4), 1829-1839. doi:10.4049/jimmunol.0902103

Chen, L., & Flies, D. B. (2013). Molecular mechanisms of T cell co-stimulation and co-inhibition. *Nature Reviews Immunology, 13*(4), 227-242.

924 Conley, J. M., Gallagher, M. P., & Berg, L. J. (2016). T Cells and Gene Regulation: The
925 Switching On and Turning Up of Genes after T Cell Receptor Stimulation in CD8 T
926 Cells. *Front Immunol, 7*, 76. doi:10.3389/fimmu.2016.00076
927 Courtney, A. H., Lo, W. L., & Weiss, A. (2018). TCR Signaling: Mechanisms of Initiation and
928 Propagation. *Trends Biochem Sci, 43*(2), 108-123. doi:10.1016/j.tibs.2017.11.008
929 Curtsinger, J. M., Johnson, C. M., & Mescher, M. F. (2003). CD8 T cell clonal expansion and
930 development of effector function require prolonged exposure to antigen,
931 costimulation, and signal 3 cytokine. *The Journal of Immunology, 171*(10), 5165-
932 5171.
933 Curtsinger, J. M., & Mescher, M. F. (2010). Inflammatory cytokines as a third signal for T cell
934 activation. *Current opinion in immunology, 22*(3), 333-340.
935 D'Oro, U., & Ashwell, J. D. (1999). Cutting edge: the CD45 tyrosine phosphatase is an
936 inhibitor of Lck activity in thymocytes. *J Immunol, 162*(4), 1879-1883.
937 Daniels, M. A., Teixeiro, E., Gill, J., Hausmann, B., Roubaty, D., Holmberg, K., Werlen, G.,
938 Hollander, G. A., Gascoigne, N. R., & Palmer, E. (2006). Thymic selection threshold
939 defined by compartmentalization of Ras/MAPK signalling. *Nature, 444*(7120), 724-
940 729. doi:10.1038/nature05269
941 Das, D. K., Feng, Y., Mallis, R. J., Li, X., Keskin, D. B., Hussey, R. E., Brady, S. K., Wang, J. H.,
942 Wagner, G., Reinherz, E. L., & Lang, M. J. (2015). Force-dependent transition in the T-
943 cell receptor beta-subunit allosterically regulates peptide discrimination and pMHC
944 bond lifetime. *Proc Natl Acad Sci U S A, 112*(5), 1517-1522.
945 doi:10.1073/pnas.1424829112
946 Das, J., Ho, M., Zikherman, J., Govern, C., Yang, M., Weiss, A., Chakraborty, A. K., & Roose, J.
947 P. (2009). Digital signaling and hysteresis characterize ras activation in lymphoid
948 cells. *Cell, 136*(2), 337-351.
949 Davis, S. J., & van der Merwe, P. A. (2006). The kinetic-segregation model: TCR triggering
950 and beyond. *Nature immunology, 7*(8), 803.
951 Delgoffe, G. M., Pollizzi, K. N., Waickman, A. T., Heikamp, E., Meyers, D. J., Horton, M. R.,
952 Xiao, B., Worley, P. F., & Powell, J. D. (2011). The kinase mTOR regulates the
953 differentiation of helper T cells through the selective activation of signaling by
954 mTORC1 and mTORC2. *Nat Immunol, 12*(4), 295-303. doi:10.1038/ni.2005
955 Denton, A. E., Wesselingh, R., Gras, S., Guillonneau, C., Olson, M. R., Mintern, J. D., Zeng, W.,
956 Jackson, D. C., Rossjohn, J., Hodgkin, P. D., Doherty, P. C., & Turner, S. J. (2011).
957 Affinity thresholds for naive CD8+ CTL activation by peptides and engineered
958 influenza A viruses. *J Immunol, 187*(11), 5733-5744. doi:10.4049/jimmunol.1003937
959 Dushek, O., Das, R., & Coombs, D. (2009). A role for rebinding in rapid and reliable T cell
960 responses to antigen. *PLoS computational biology, 5*(11), e1000578.
961 Dustin, M. L., & Springer, T. A. (1989). T-cell receptor cross-linking transiently stimulates
962 adhesiveness through LFA-1. *Nature, 341*(6243), 619-624.
963 Esensten, J. H., Helou, Y. A., Chopra, G., Weiss, A., & Bluestone, J. A. (2016). CD28
964 costimulation: from mechanism to therapy. *Immunity, 44*(5), 973-988.
965 Ferrell, J. E., Jr., & Ha, S. H. (2014). Ultrasensitivity part I: Michaelian responses and zero-
966 order ultrasensitivity. *Trends Biochem Sci, 39*(10), 496-503.
967 doi:10.1016/j.tibs.2014.08.003
968 Gérard, A., Khan, O., Beemiller, P., Oswald, E., Hu, J., Matloubian, M., & Krummel, M. F.
969 (2013). Secondary T cell–T cell synaptic interactions drive the differentiation of
970 protective CD8+ T cells. *Nature immunology, 14*(4), 356.

971 Goldbeter, A., & Koshland, D. E. (1981). An amplified sensitivity arising from covalent
972 modification in biological systems. *Proceedings of the national academy of sciences,*
973 *78*(11), 6840-6844.
974 Gopalakrishnan, M. J. F. (2019). ncdfFlow: ncdfFlow: A package that provides HDF5 based
975 storage for flow cytometry data. R package version 2.33.0.
976 Hahne, F., LeMeur, N., Brinkman, R. R., Ellis, B., Haaland, P., Sarkar, D., Spidlen, J., Strain, E.,
977 & Gentleman, R. (2009). flowCore: a Bioconductor package for high throughput flow
978 cytometry. *BMC Bioinformatics, 10*, 106. doi:10.1186/1471-2105-10-106
979 Heinzel, S., Giang, T. B., Kan, A., Marchingo, J. M., Lye, B. K., Corcoran, L. M., & Hodgkin, P.
980 D. (2017). A Myc-dependent division timer complements a cell-death timer to
981 regulate T cell and B cell responses. *Nature immunology, 18*(1), 96-103.
982 Hogquist, K. A., Jameson, S. C., Heath, W. R., Howard, J. L., Bevan, M. J., & Carbone, F. R.
983 (1994). T cell receptor antagonist peptides induce positive selection. *Cell, 76*(1), 17-
984 27. doi:10.1016/0092-8674(94)90169-4
985 Hommel, M., & Hodgkin, P. D. (2007). TCR affinity promotes CD8+ T cell expansion by
986 regulating survival. *J Immunol, 179*(4), 2250-2260. doi:10.4049/jimmunol.179.4.2250
987 Hong, J., Ge, C., Jothikumar, P., Yuan, Z., Liu, B., Bai, K., Li, K., Rittase, W., Shinzawa, M.,
988 Zhang, Y., Palin, A., Love, P., Yu, X., Salaita, K., Evavold, B. D., Singer, A., & Zhu, C.
989 (2018). A TCR mechanotransduction signaling loop induces negative selection in the
990 thymus. *Nat Immunol, 19*(12), 1379-1390. doi:10.1038/s41590-018-0259-z
991 Howden, A. J. M., Hukelmann, J. L., Brenes, A., Spinelli, L., Sinclair, L. V., Lamond, A. I., &
992 Cantrell, D. A. (2019). Quantitative analysis of T cell proteomes and environmental
993 sensors during T cell differentiation. *Nat Immunol*. doi:10.1038/s41590-019-0495-x
994 Huang, W. Y. C., Alvarez, S., Kondo, Y., Lee, Y. K., Chung, J. K., Lam, H. Y. M., Biswas, K. H.,
995 Kuriyan, J., & Groves, J. T. (2019). A molecular assembly phase transition and kinetic
996 proofreading modulate Ras activation by SOS. *Science, 363*(6431), 1098-1103.
997 doi:10.1126/science.aau5721
998 Hubo, M., Trinschek, B., Kryczanowsky, F., Tuettenberg, A., Steinbrink, K., & Jonuleit, H.
999 (2013). Costimulatory molecules on immunogenic versus tolerogenic human
1000 dendritic cells. *Frontiers in immunology, 4*, 82.
1001 Hui, E., & Vale, R. D. (2014). In vitro membrane reconstitution of the T-cell receptor
1002 proximal signaling network. *Nature structural & molecular biology, 21*(2), 133.
1003 Iezzi, G., Karjalainen, K., & Lanzavecchia, A. (1998). The duration of antigenic stimulation
1004 determines the fate of naive and effector T cells. *Immunity, 8*(1), 89-95.
1005 James, J. R. (2018). Tuning ITAM multiplicity on T cell receptors can control potency and
1006 selectivity to ligand density. *Sci Signal, 11*(531). doi:10.1126/scisignal.aan1088
1007 Jenkins, M. K., & Moon, J. J. (2012). The role of naive T cell precursor frequency and
1008 recruitment in dictating immune response magnitude. *J Immunol, 188*(9), 4135-
1009 4140. doi:10.4049/jimmunol.1102661
1010 Juang, J., Ebert, P. J., Feng, D., Garcia, K. C., Krogsgaard, M., & Davis, M. M. (2010). Peptide-
1011 MHC heterodimers show that thymic positive selection requires a more restricted
1012 set of self-peptides than negative selection. *J Exp Med, 207*(6), 1223-1234.
1013 doi:10.1084/jem.20092170
1014 Kaech, S. M., & Ahmed, R. (2001). Memory CD8+ T cell differentiation: initial antigen
1015 encounter triggers a developmental program in naive cells. *Nature immunology,*
1016 *2*(5), 415-422.

Kannan, A., Huang, W., Huang, F., & August, A. (2012). Signal transduction via the T cell antigen receptor in naive and effector/memory T cells. *Int J Biochem Cell Biol, 44*(12), 2129-2134. doi:10.1016/j.biocel.2012.08.023

Kedia-Mehta, N., & Finlay, D. K. (2019). Competition for nutrients and its role in controlling immune responses. *Nature communications, 10*(1), 1-8.

King, C. G., Koehli, S., Hausmann, B., Schmaler, M., Zehn, D., & Palmer, E. (2012). T cell affinity regulates asymmetric division, effector cell differentiation, and tissue pathology. *Immunity, 37*(4), 709-720. doi:10.1016/j.immuni.2012.06.021

Kingeter, L. M., Paul, S., Maynard, S. K., Cartwright, N. G., & Schaefer, B. C. (2010). Cutting edge: TCR ligation triggers digital activation of NF-kappaB. *J Immunol, 185*(8), 4520-4524. doi:10.4049/jimmunol.1001051

Krishnaswamy, S., Spitzer, M. H., Mingueneau, M., Bendall, S. C., Litvin, O., Stone, E., Pe'er, D., & Nolan, G. P. (2014). Systems biology. Conditional density-based analysis of T cell signaling in single-cell data. *Science, 346*(6213), 1250689. doi:10.1126/science.1250689

Le Borgne, M., Raju, S., Zinselmeyer, B. H., Le, V. T., Li, J., Wang, Y., Miller, M. J., & Shaw, A. S. (2016). Real-time analysis of calcium signals during the early phase of T cell activation using a genetically encoded calcium biosensor. *J Immunol, 196*(4), 1471-1479. doi:10.4049/jimmunol.1502414

Lee, P. A., Wallace, E., Marlow, A., Yeh, T., Marsh, V., Anderson, D., Woessner, R., Hurley, B., Lyssikatos, J., & Poch, G. (2010). Preclinical development of ARRY-162, a potent and selective MEK 1/2 inhibitor. *Cancer Res, 70*(1), abstract 2515.

Limozin, L., Bridge, M., Bongrand, P., Dushek, O., van der Merwe, P. A., & Robert, P. (2019). TCR-pMHC kinetics under force in a cell-free system show no intrinsic catch bond, but a minimal encounter duration before binding. *Proc Natl Acad Sci U S A, 116*(34), 16943-16948. doi:10.1073/pnas.1902141116

Liu, B., Chen, W., Evavold, B. D., & Zhu, C. (2014). Accumulation of dynamic catch bonds between TCR and agonist peptide-MHC triggers T cell signaling. *Cell, 157*(2), 357-368.

Lo, W. L., Shah, N. H., Rubin, S. A., Zhang, W., Horkova, V., Fallahee, I. R., Stepanek, O., Zon, L. I., Kuriyan, J., & Weiss, A. (2019). Slow phosphorylation of a tyrosine residue in LAT optimizes T cell ligand discrimination. *Nat Immunol*. doi:10.1038/s41590-019-0502-2

Lou, X., Zhang, G., Herrera, I., Kinach, R., Ornatsky, O., Baranov, V., Nitz, M., & Winnik, M. A. (2007). Polymer-based elemental tags for sensitive bioassays. *Angew Chem Int Ed Engl, 46*(32), 6111-6114. doi:10.1002/anie.200700796

Lun, A. T., Chen, Y., & Smyth, G. K. (2016). It's DE-licious: a recipe for differential expression analyses of RNA-seq experiments using quasi-likelihood methods in edgeR. In *Statistical Genomics* (pp. 391-416): Springer.

Lun, A. T. L., Richard, A. C., & Marioni, J. C. (2017). Testing for differential abundance in mass cytometry data. *Nat Methods, 14*(7), 707-709. doi:10.1038/nmeth.4295

Marchingo, J. M., Kan, A., Sutherland, R. M., Duffy, K. R., Wellard, C. J., Belz, G. T., Lew, A. M., Dowling, M. R., Heinzel, S., & Hodgkin, P. D. (2014). Antigen affinity, costimulation, and cytokine inputs sum linearly to amplify T cell expansion. *Science, 346*(6213), 1123-1127.

Marth, J. D., Cooper, J. A., King, C. S., Ziegler, S. F., Tinker, D. A., Overell, R. W., Krebs, E. G., & Perlmutter, R. M. (1988). Neoplastic transformation induced by an activated lymphocyte-specific protein tyrosine kinase (pp56lck). *Mol Cell Biol, 8*(2), 540-550. doi:10.1128/mcb.8.2.540

McKeithan, T. W. (1995). Kinetic proofreading in T-cell receptor signal transduction. *Proceedings of the national academy of sciences, 92*(11), 5042-5046.

Mingueneau, M., Krishnaswamy, S., Spitzer, M. H., Bendall, S. C., Stone, E. L., Hedrick, S. M., Pe'er, D., Mathis, D., Nolan, G. P., & Benoist, C. (2014). Single-cell mass cytometry of TCR signaling: amplification of small initial differences results in low ERK activation in NOD mice. *Proc Natl Acad Sci U S A, 111*(46), 16466-16471. doi:10.1073/pnas.1419337111

Moran, A. E., Holzapfel, K. L., Xing, Y., Cunningham, N. R., Maltzman, J. S., Punt, J., & Hogquist, K. A. (2011). T cell receptor signal strength in Treg and iNKT cell development demonstrated by a novel fluorescent reporter mouse. *J Exp Med, 208*(6), 1279-1289. doi:10.1084/jem.20110308

Moreau, H. D., Lemaitre, F., Terriac, E., Azar, G., Piel, M., Lennon-Dumenil, A. M., & Bousso, P. (2012). Dynamic in situ cytometry uncovers T cell receptor signaling during immunological synapses and kinapses in vivo. *Immunity, 37*(2), 351-363. doi:10.1016/j.immuni.2012.05.014

Mukhopadhyay, H., de Wet, B., Clemens, L., Maini, P. K., Allard, J., van der Merwe, P. A., & Dushek, O. (2016). Multisite Phosphorylation Modulates the T Cell Receptor zeta-Chain Potency but not the Switchlike Response. *Biophys J, 110*(8), 1896-1906. doi:10.1016/j.bpj.2016.03.024

Navarro, M. N., & Cantrell, D. A. (2014). Serine-threonine kinases in TCR signaling. *Nat Immunol, 15*(9), 808-814. doi:10.1038/ni.2941

Navarro, M. N., Feijoo-Carnero, C., Arandilla, A. G., Trost, M., & Cantrell, D. A. (2014). Protein kinase D2 is a digital amplifier of T cell receptor-stimulated diacylglycerol signaling in naive CD8(+) T cells. *Sci Signal, 7*(348), ra99. doi:10.1126/scisignal.2005477

Nelson, N., Kanno, Y., Hong, C., Contursi, C., Fujita, T., Fowlkes, B. J., O'Connell, E., Hu-Li, J., Paul, W. E., Jankovic, D., Sher, A. F., Coligan, J. E., Thornton, A., Appella, E., Yang, Y., & Ozato, K. (1996). Expression of IFN regulatory factor family proteins in lymphocytes. Induction of Stat-1 and IFN consensus sequence binding protein expression by T cell activation. *J Immunol, 156*(10), 3711-3720.

Ornatsky, O., Bandura, D., Baranov, V., Nitz, M., Winnik, M. A., & Tanner, S. (2010). Highly multiparametric analysis by mass cytometry. *J Immunol Methods, 361*(1-2), 1-20. doi:10.1016/j.jim.2010.07.002

Ozga, A. J., Moalli, F., Abe, J., Swoger, J., Sharpe, J., Zehn, D., Kreutzfeldt, M., Merkler, D., Ripoll, J., & Stein, J. V. (2016). pMHC affinity controls duration of CD8+ T cell-DC interactions and imprints timing of effector differentiation versus expansion. *J Exp Med, 213*(12), 2811-2829. doi:10.1084/jem.20160206

Palmer, E., Drobek, A., & Stepanek, O. (2016). Opposing effects of actin signaling and LFA-1 on establishing the affinity threshold for inducing effector T-cell responses in mice. *Eur J Immunol, 46*(8), 1887-1901. doi:10.1002/eji.201545909

Paul, S., & Schaefer, B. C. (2013). A new look at T cell receptor signaling to nuclear factor-kappaB. *Trends Immunol, 34*(6), 269-281. doi:10.1016/j.it.2013.02.002

Pende, M., Um, S. H., Mieulet, V., Sticker, M., Goss, V. L., Mestan, J., Mueller, M., Fumagalli, S., Kozma, S. C., & Thomas, G. (2004). S6K1(-/-)/S6K2(-/-) mice exhibit perinatal lethality and rapamycin-sensitive 5'-terminal oligopyrimidine mRNA translation and reveal a mitogen-activated protein kinase-dependent S6 kinase pathway. *Mol Cell Biol, 24*(8), 3112-3124. doi:10.1128/mcb.24.8.3112-3124.2004

1111 Pipkin, M. E., Sacks, J. A., Cruz-Guilloty, F., Lichtenheld, M. G., Bevan, M. J., & Rao, A. (2010).
1112 Interleukin-2 and inflammation induce distinct transcriptional programs that
1113 promote the differentiation of effector cytolytic T cells. *Immunity, 32*(1), 79-90.
1114 Pollizzi, K. N., & Powell, J. D. (2015). Regulation of T cells by mTOR: the known knowns and
1115 the known unknowns. *Trends Immunol, 36*(1), 13-20. doi:10.1016/j.it.2014.11.005
1116 Prasad, A., Zikherman, J., Das, J., Roose, J. P., Weiss, A., & Chakraborty, A. K. (2009). Origin
1117 of the sharp boundary that discriminates positive and negative selection of
1118 thymocytes. *Proc Natl Acad Sci U S A, 106*(2), 528-533.
1119 doi:10.1073/pnas.0805981105
1120 Prlic, M., Hernandez-Hoyos, G., & Bevan, M. J. (2006). Duration of the initial TCR stimulus
1121 controls the magnitude but not functionality of the CD8+ T cell response. *The Journal
1122 of experimental medicine, 203*(9), 2135-2143.
1123 Razvag, Y., Neve-Oz, Y., Sajman, J., Reches, M., & Sherman, E. (2018). Nanoscale kinetic
1124 segregation of TCR and CD45 in engaged microvilli facilitates early T cell activation.
1125 *Nature communications, 9*(1), 732.
1126 Richard, A. C., Lun, A. T. L., Lau, W. W. Y., Gottgens, B., Marioni, J. C., & Griffiths, G. M.
1127 (2018). T cell cytolytic capacity is independent of initial stimulation strength. *Nat
1128 Immunol, 19*(8), 849-858. doi:10.1038/s41590-018-0160-9
1129 Robinson, M. D., McCarthy, D. J., & Smyth, G. K. (2010). edgeR: a Bioconductor package for
1130 differential expression analysis of digital gene expression data. *Bioinformatics, 26*(1),
1131 139-140. doi:10.1093/bioinformatics/btp616
1132 Rosette, C., Werlen, G., Daniels, M. A., Holman, P. O., Alam, S. M., Travers, P. J., Gascoigne,
1133 N. R., Palmer, E., & Jameson, S. C. (2001). The impact of duration versus extent of
1134 TCR occupancy on T cell activation: a revision of the kinetic proofreading model.
1135 *Immunity, 15*(1), 59-70. doi:10.1016/s1074-7613(01)00173-x
1136 Ross, S. H., Rollings, C., Anderson, K. E., Hawkins, P. T., Stephens, L. R., & Cantrell, D. A.
1137 (2016). Phosphoproteomic analyses of interleukin 2 signaling reveal integrated JAK
1138 kinase-dependent and-independent networks in CD8+ T cells. *Immunity, 45*(3), 685-
1139 700.
1140 Roux, P. P., Shahbazian, D., Vu, H., Holz, M. K., Cohen, M. S., Taunton, J., Sonenberg, N., &
1141 Blenis, J. (2007). RAS/ERK signaling promotes site-specific ribosomal protein S6
1142 phosphorylation via RSK and stimulates cap-dependent translation. *J Biol Chem,
1143 282*(19), 14056-14064. doi:10.1074/jbc.M700906200
1144 Ryu, H., Chung, M., Song, J., Lee, S. S., Pertz, O., & Jeon, N. L. (2018). Integrated platform for
1145 monitoring single-cell MAPK kinetics in computer-controlled temporal stimulations.
1146 *Sci Rep, 8*(1), 11126. doi:10.1038/s41598-018-28873-1
1147 Salmond, R. J. (2018). mTOR regulation of glycolytic metabolism in T cells. *Front Cell Dev
1148 Biol, 6*, 122. doi:10.3389/fcell.2018.00122
1149 Salmond, R. J., Brownlie, R. J., Meyuhas, O., & Zamoyska, R. (2015). Mechanistic target of
1150 rapamycin complex 1/S6 kinase 1 signals influence T cell activation independently of
1151 ribosomal protein S6 phosphorylation. *J Immunol, 195*(10), 4615-4622.
1152 doi:10.4049/jimmunol.1501473
1153 Salmond, R. J., Brownlie, R. J., Morrison, V. L., & Zamoyska, R. (2014). The tyrosine
1154 phosphatase PTPN22 discriminates weak self peptides from strong agonist TCR
1155 signals. *Nature immunology, 15*(9), 875.
1156 Salmond, R. J., Emery, J., Okkenhaug, K., & Zamoyska, R. (2009). MAPK, phosphatidylinositol
1157 3-kinase, and mammalian target of rapamycin pathways converge at the level of

ribosomal protein S6 phosphorylation to control metabolic signaling in CD8 T cells. *J Immunol, 183*(11), 7388-7397. doi:10.4049/jimmunol.0902294

Sarbassov, D. D., Ali, S. M., Sengupta, S., Sheen, J. H., Hsu, P. P., Bagley, A. F., Markhard, A. L., & Sabatini, D. M. (2006). Prolonged rapamycin treatment inhibits mTORC2 assembly and Akt/PKB. *Mol Cell, 22*(2), 159-168. doi:10.1016/j.molcel.2006.03.029

Sibener, L. V., Fernandes, R. A., Kolawole, E. M., Carbone, C. B., Liu, F., McAffee, D., Birnbaum, M. E., Yang, X., Su, L. F., Yu, W., Dong, S., Gee, M. H., Jude, K. M., Davis, M. M., Groves, J. T., Goddard, W. A., 3rd, Heath, J. R., Evavold, B. D., Vale, R. D., & Garcia, K. C. (2018). Isolation of a structural mechanism for uncoupling T cell receptor signaling from peptide-MHC binding. *Cell, 174*(3), 672-687 e627. doi:10.1016/j.cell.2018.06.017

Tan, T. C. J., Knight, J., Sbarrato, T., Dudek, K., Willis, A. E., & Zamoyska, R. (2017). Suboptimal T-cell receptor signaling compromises protein translation, ribosome biogenesis, and proliferation of mouse CD8 T cells. *Proc Natl Acad Sci U S A, 114*(30), E6117-E6126. doi:10.1073/pnas.1700939114

Tian, T., Harding, A., Inder, K., Plowman, S., Parton, R. G., & Hancock, J. F. (2007). Plasma membrane nanoswitches generate high-fidelity Ras signal transduction. *Nat Cell Biol, 9*(8), 905-914. doi:10.1038/ncb1615

van Stipdonk, M. J., Hardenberg, G., Bijker, M. S., Lemmens, E. E., Droin, N. M., Green, D. R., & Schoenberger, S. P. (2003). Dynamic programming of CD8+ T lymphocyte responses. *Nature immunology, 4*(4), 361-365.

van Stipdonk, M. J., Lemmens, E. E., & Schoenberger, S. P. (2001). Naive CTLs require a single brief period of antigenic stimulation for clonal expansion and differentiation. *Nature immunology, 2*(5), 423-429.

Verdeil, G., Puthier, D., Nguyen, C., Schmitt-Verhulst, A.-M., & Auphan-Anezin, N. (2006). STAT5-mediated signals sustain a TCR-initiated gene expression program toward differentiation of CD8 T cell effectors. *The Journal of Immunology, 176*(8), 4834-4842.

Verma, N. K., & Kelleher, D. (2017). Not just an adhesion molecule: LFA-1 contact tunes the T lymphocyte program. *The Journal of Immunology, 199*(4), 1213-1221.

Voisinne, G., Kersse, K., Chaoui, K., Lu, L., Chaix, J., Zhang, L., Goncalves Menoita, M., Girard, L., Ounoughene, Y., Wang, H., Burlet-Schiltz, O., Luche, H., Fiore, F., Malissen, M., Gonzalez de Peredo, A., Liang, Y., Roncagalli, R., & Malissen, B. (2019). Quantitative interactomics in primary T cells unveils TCR signal diversification extent and dynamics. *Nat Immunol*. doi:10.1038/s41590-019-0489-8

Voisinne, G., Nixon, B. G., Melbinger, A., Gasteiger, G., Vergassola, M., & Altan-Bonnet, G. (2015). T cells integrate local and global cues to discriminate between structurally similar antigens. *Cell reports, 11*(8), 1208-1219.

Wensveen, F. M., van Gisbergen, K. P., & Eldering, E. (2012). The fourth dimension in immunological space: how the struggle for nutrients selects high - affinity lymphocytes. *Immunological reviews, 249*(1), 84-103.

Wolchinsky, R., Hod-Marco, M., Oved, K., Shen-Orr, S. S., Bendall, S. C., Nolan, G. P., & Reiter, Y. (2014). Antigen-dependent integration of opposing proximal TCR-signaling cascades determines the functional fate of T lymphocytes. *J Immunol, 192*(5), 2109-2119. doi:10.4049/jimmunol.1301142

Wong, P., & Pamer, E. G. (2001). Cutting edge: antigen-independent CD8 T cell proliferation. *The Journal of Immunology, 166*(10), 5864-5868.

Wu, J., Katrekar, A., Honigberg, L. A., Smith, A. M., Conn, M. T., Tang, J., Jeffery, D., Mortara, K., Sampang, J., & Williams, S. R. (2006). Identification of substrates of human protein-tyrosine phosphatase PTPN22. *Journal of Biological Chemistry, 281*(16), 11002-11010.

Wu, P., Zhang, T., Liu, B., Fei, P., Cui, L., Qin, R., Zhu, H., Yao, D., Martinez, R. J., Hu, W., An, C., Zhang, Y., Liu, J., Shi, J., Fan, J., Yin, W., Sun, J., Zhou, C., Zeng, X., Xu, C., Wang, J., Evavold, B. D., Zhu, C., Chen, W., & Lou, J. (2019). Mechano-regulation of Peptide-MHC Class I Conformations Determines TCR Antigen Recognition. *Mol Cell, 73*(5), 1015-1027 e1017. doi:10.1016/j.molcel.2018.12.018

Wulfing, C., Rabinowitz, J. D., Beeson, C., Sjaastad, M. D., McConnell, H. M., & Davis, M. M. (1997). Kinetics and extent of T cell activation as measured with the calcium signal. *J Exp Med, 185*(10), 1815-1825. doi:10.1084/jem.185.10.1815

Yang, W., Pan, W., Chen, S., Trendel, N., Jiang, S., Xiao, F., Xue, M., Wu, W., Peng, Z., & Li, X. (2017). Dynamic regulation of CD28 conformation and signaling by charged lipids and ions. *Nature structural & molecular biology, 24*(12), 1081.

Zehn, D., Lee, S. Y., & Bevan, M. J. (2009). Complete but curtailed T-cell response to very low-affinity antigen. *Nature, 458*(7235), 211-214. doi:10.1038/nature07657

Zikherman, J., & Au-Yeung, B. (2015). The role of T cell receptor signaling thresholds in guiding T cell fate decisions. *Curr Opin Immunol, 33*, 43-48. doi:10.1016/j.coi.2015.01.012

Figure Legends:

Figure 1: Diagrammatic representation of TCR signalling pathways measured by mass cytometry panel

Cartoon depicts the TCR-related signalling pathways examined in this study in our minimal stimulation system wherein T cells present antigen to each other. Solid lines indicate evidence of direct and dotted lines suggested or indirect interaction. Signalling proteins and post-translational modifications directly measured by mass cytometry antibodies are outlined in purple. The mass cytometry panel also profiled surface proteins TCRβ, CD8α, CD45, CD25 (IL2Rα), and CD44.

Figure 2. Mass cytometry measurements of signalling events in singlet and doublet events.

a) Naïve $CD8^+$ T cells were stimulated with 1 μM peptides of various potencies for 0, 1, 2, 4 and 6h before profiling by mass cytometry. Histograms depict pS6 signal. b) Bubble plots of all signalling molecules after stimulation as in (a) in mass cytometry events with 1 or 2 cell-equivalents of DNA (singlets or doublets, respectively). The size of the bubbles denotes the percentage of positive cells, and the colour denotes the centred and scaled median intensity of each positive fraction. Results are representative of cells from 6 biological replicates measured in 2 independent experiments as detailed in Supplementary File 1.

The following figure supplements are available for figure 2.

Figure 2- figure supplement 1. Titrating peptide concentration.

Figure 2- figure supplement 2. Gating based on DNA content and comparison of signalling markers.

Figure 3. Kinetics of selected signalling proteins and impact of MEK and mTOR pathway inhibitors on T cell activation parameters.

a) The percentage of cells positive for each marker is plotted against time. Results depict combined data from 6 biological replicates measured in 2 independent experiments as detailed in Supplementary File 1. Points represent the mean and error bars depict the SD. Data underlying plots are provided in Supplementary File 5. b-c) Flow cytometry measurements of pS6[S235/236] and pERK1/2 after 2h of pre-treatment with DMSO vehicle control, rapamycin (Rapa) 200 nM, MEK162 (MEK) 0.5 µM, 1 µM and 5 µM, or combined rapamycin with MEK162 (R + M), followed by 4h stimulation with 1 µM N4 or NP68 peptides. Results are representative of 3 independent experiments. d) The fraction of $pS6^{+}$ cells in N4-stimulated conditions with the indicated inhibitor treatments versus DMSO (top). The median fluorescent intensity of pS6 among $pS6^{+}$ cells in N4-stimulated conditions with the indicated inhibitor treatments (bottom). Lines represent the median. Results depict combined data from 3 independent experiments.

The following figure supplements are available for figure 3.

Figure 3- figure supplement 1. Kinetics of total protein levels and surface markers.

Figure 3- figure supplement 2. Kinetics of pSTAT5, pLCK and pSLP76 signalling proteins, and testing the impact of IL2.

Figure 3- figure supplement 3. pERK and pS6 distributions and additional MEK and mTOR inhibition data.

Figure 4. Examination of multi-dimensional phenotypes in mass cytometry signalling data.

a) Mass cytometry stimulation time courses were further investigated for multidimensional phenotypes that changed in abundance with stimulation. Analysis was run on 2 multiplexed biological replicates as described in Methods. Phenotypic hyperspheres were defined within the multidimensional mass cytometry space and abundances of cells from each condition enumerated within each hypersphere. Each column in the heatmap represents an individual hypersphere. At the top of the heatmap, rows correspond to mass cytometry marker measurements with colour depicting the intensity of each marker in each hypersphere. Clustering by Pearson correlation was performed on these hypersphere marker intensity measurements. At the bottom of the heatmap, rows correspond to stimulation conditions with colour depicting the binned $\log_2$-fold change in cellular abundance in stimulated versus unstimulated conditions within each hypersphere. ns = hyperspheres that did not significantly change in abundance. Phenotypic clusters of interest, A, A', B, B', are indicated in both $CD44^+$ and $CD44^-$ populations by coloured highlighting of the dendrogram. Statistics underlying the heatmap are provided in Supplementary File 5. b) Percentages of cells exhibiting A, A', B, and B' phenotypes in mass cytometry measurements. Results are combined data from 6 biological replicates measured in 2 independent experiments as detailed in Supplementary File 1. Points represent the mean and error bars depict the SD. Data underlying plots are provided in Supplementary File 5. c) Phenotypes as in (b) further sub-divided by CD44 expression.

The following figure supplements are available for figure 4.

Figure 4- figure supplement 1. t-SNE visualization of significantly differentially abundant hyperspheres.

Figure 4- figure supplement 2. Heatmap of populations in Figure 4c additionally including $pS6^-$ populations.

Figure 5. Cartoon Model

Cartoon depicts the kinetics of the 4 main signalling phenotypes in cells stimulated with ligands of varying potencies (N4, T4, G4) over time from data in Figures 3A and 4A-B (note the transient $pERK^+$ populations, even with G4). Black outlines indicate $CD44^+$ populations.

The following figure supplements are available for figure 5.

Figure 5- figure supplement 1. Activation trajectories for examining the order of signalling events.

***Figure 6. Simultaneous measurement of phosphorylation of S6 and mRNA expression of transcription factors Nr4a1 and Irf8*.**

a) Combined phosphoflow cytometry of pS6 and RNA flow cytometry of *Nr4a1* and *Irf8* transcripts in naïve OT-I $CD8^+$ T cells stimulated with N4, T4, G4 or NP68 peptides for 2h, gated on single live cells in which the control gene *Rpl39* was detected. b) Frequency of

phenotypes depicted in (a) after stimulation for 1, 2, 4 or 6h. Data are representative of 3 independent experiments.

The following figure supplements are available for figure 6.

Figure 6- figure supplement 1. RNA flow cytometry gating strategy and histograms.

Figure 7. Signalling phenotypes in T cells stimulated with peptide-pulsed APCs

a) Naïve $CD8^+$ T cells were stimulated with mature BMDCs loaded with peptides of various potencies for 1, 2, 4 and 6h before profiling by flow cytometry. The percentage of cells positive for each marker is plotted against time. Results depict combined data from 3 independent experiments. Points represent the mean and error bars depict the SD. b) Example flow cytometry data from (a) of pERK1/2 and pS6 measured at 1 and 6h.

Figure 7 – source data 1. Data underlying plots in Figure 7a.

The following figure supplements are available for figure 7.

Figure 7- figure supplement 1. Expression of adhesion and costimulatory molecules on T cells and BMDCs.

Figure Supplement Legends

Figure 2- figure supplement 1: Titrating peptide concentration

a) Flow cytometry measurements of pS6 and pERK after 2 or 4h of simulation with 10 nM, 100 nM or 1 µM of N4, T4, G4 or NP68 peptides. Results are representative of 3 biological replicates.

Figure 2- figure supplement 2: Gating based on DNA content and comparison of signalling markers

a) Gating strategy used to select mass cytometry events containing one or two cell-equivalents of DNA from mass cytometry data in Figure 2. b) Percentages of mass cytometry events deemed doublets (2 cell-equivalents of DNA). Plot depicts mean and standard deviation of 6 biological replicates measured in 2 independent experiments as detailed in Supplementary File 1. c-d) Expression of total (c) and phosphorylated (d) protein measurements in cells stimulated with N4 peptide for 1h, gated on singlets (red) versus doublets (blue). Data is representative of 6 biological replicates measured in 2 independent experiments. e) As (d) after normalization of signalling molecules to total DNA levels.

Figure 3- figure supplement 1: Kinetics of total protein levels and surface markers

The median intensity of proteins measured by mass cytometry under stimulation with ligands of various potencies over time. Points represent the mean and error bars depict the

SD. Results depict combined data from 6 biological replicates measured in 2 independent experiments as detailed in Supplementary File 1.

Figure 3 – figure supplement 2: Kinetics of pSTAT5, pLCK and pSLP76 signalling proteins and testing the impact of IL2.

a) As Figure 3a for pSTAT5, pLCK and pSLP76. Plots depict combined data from 6 biological replicates measured in 2 independent experiments as detailed in Supplementary File 1. Points represent the mean and error bars depict the SD. Data underlying plots are provided in Supplementary File 1. b) Flow cytometry measurements of pSTAT5, pS6[S235/236] pERK1/2, pAKT and IκBα, stimulated with peptides of various potencies for 4h, in the presence or absence of IL2. Results depict combined data from 3 biological replicates measured in 2-3 independent experiments. Bar charts represent the mean and error bars depict the SD.

Figure 3 – figure supplement 3: pERK and pS6 distributions and additional MEK and mTOR inhibition data

a) Cells were gated on pERK1/2 positive and negative populations. Within these populations, the median marker intensity was calculated at each timepoint in each condition. b) As (a) for pS6[S235/S236]. c) As (b) after normalization of pS6 intensity to total S6 intensity within each cell. a-c) Plots are representative of 6 biological replicates measured in 2 independent experiments as detailed in Supplementary File 1. d) As Figure 3b, measuring pERK1/2. e) Flow cytometry measurements of pS6[S235/236] after stimulation in

the presence of the indicated concentrations of rapamycin. f) The median fluorescent intensity of CD44 among live cells in N4-stimulated conditions with the indicated inhibitor treatments. Results depict combined data from 3 independent experiments. Lines represent the mean. g) 2-day proliferation assay of cells treated as in (d-f) measured using Cell Proliferation Dye eFluor450. d,e,g) Results are representative of 3 biological replicates from 2-3 independent experiments.

Figure 4 – figure supplement 1: t-SNE visualization of significantly differentially abundant hyperspheres

a) tSNE plots depict hyperspheres from Figure 4a. Colour indicates log_2-fold change of cellular abundance in each stimulated condition versus unstimulated for each hypersphere. b) As (a) with colour indicating the median intensity of each marker within each hypersphere. Underlying data are provided in Supplementary File 5.

Figure 4 – figure supplement 2: Heatmap of populations in Figure 4c including pS6$^-$

Data from Figure 4c, additionally including pS6$^-$ phenotypes, are plotted as a heatmap. Plots depict averages from 6 biological replicates measured in 2 independent experiments as detailed in Supplementary File 1.

Figure 5 – figure supplement 1: Activation trajectories for examining the order of signalling events

a) Mass cytometry data was grouped by biological replicate and stimulating ligand before constructing activation trajectories by ordering the cells according to pS6 intensity. Plots depict 1000 randomly sampled cells from an example replicate. Colours represent real times at which cells were sampled. b) Example of pERK1/2 intensity measurements along the trajectories constructed in (a). c) Loess curves were fitted to intensities of the indicated markers along the trajectories depicted in (a). Dotted lines represent the estimated standard error from the loess fits. d) As (c) for additional signalling markers. Trajectories are representative of the 4 biological replicates that included at least 3 time points, measured in 2 independent experiments as detailed in Supplementary File 1.

Figure 6 – figure supplement 1: RNA flow cytometry gating strategy and histograms

a) Single cell RNA-seq of *Irf8* and *Nr4a1* expression after 0-6 hours stimulation with 1 µM N4 peptide from previously published data (Richard et al., 2018), ArrayExpress E-MTAB-6051, depicted as violin plots, with dots indicating individual cells. b) Gating strategy for combined phosphoflow cytometry of pS6 and RNA flow cytometry: cells were gated on size, single cells, live cells and *Rpl39*$^{+}$ cells, before examining *Nr4a1*, *Irf8* and pS6 with gates based on fluorescence-minus-one stains. c) As Figure 6, histograms depict flow cytometry measurements of *Nr4a1, Irf8* and pS6 (gated on *Rpl39*$^{+}$ cells), and the control mRNA *Rpl39* (gated on live cells) over all time points measured. Data are representative of 3 independent experiments.

Figure 7 – figure supplement 1: Expression of adhesion and costimulatory molecules on T cells and BMDCs

a) Expression of CD80 and ICAM-1 on T cells after 6 hours of stimulation with 1 µM of the indicated peptides. Results are representative of 3 biological replicates measured in 2 independent experiments. b) Surface protein phenotyping of BMDCs before and after maturation for 1 day with LPS. Results are representative of 5 independent experiments.

Supplementary File Legends

Supplementary File 1: Replicate structure

Table details independent experiments, biological replicates and, where applicable, barcoding strategies

Supplementary File 2: Key Resources Table

Supplementary File 3: Antibodies for mass cytometry

Supplementary File 4: Antibody testing and specificity

Antibody specificity tables detail experiments used to test and validate a) antibodies targeting total proteins and b-c) signalling proteins. Tables also include relevant references utilising these clones in knockout, knockdown, overexpression or small molecule inhibitor experiments.

Supplementary File 5: Mass cytometry figure underlying data

Tables provide means and standard deviations of kinetics curves depicted in Figures 3a, 4b-c, and Figure 3 – figure supplement 2a, as well as summary statistics from hypersphere differential abundance testing depicted in Figure 4a and Figure 4 – figure supplement 1.

Source Data Files

Figure 7 – source data 1. Data underlying plots in Figure 7a.

Figure 1

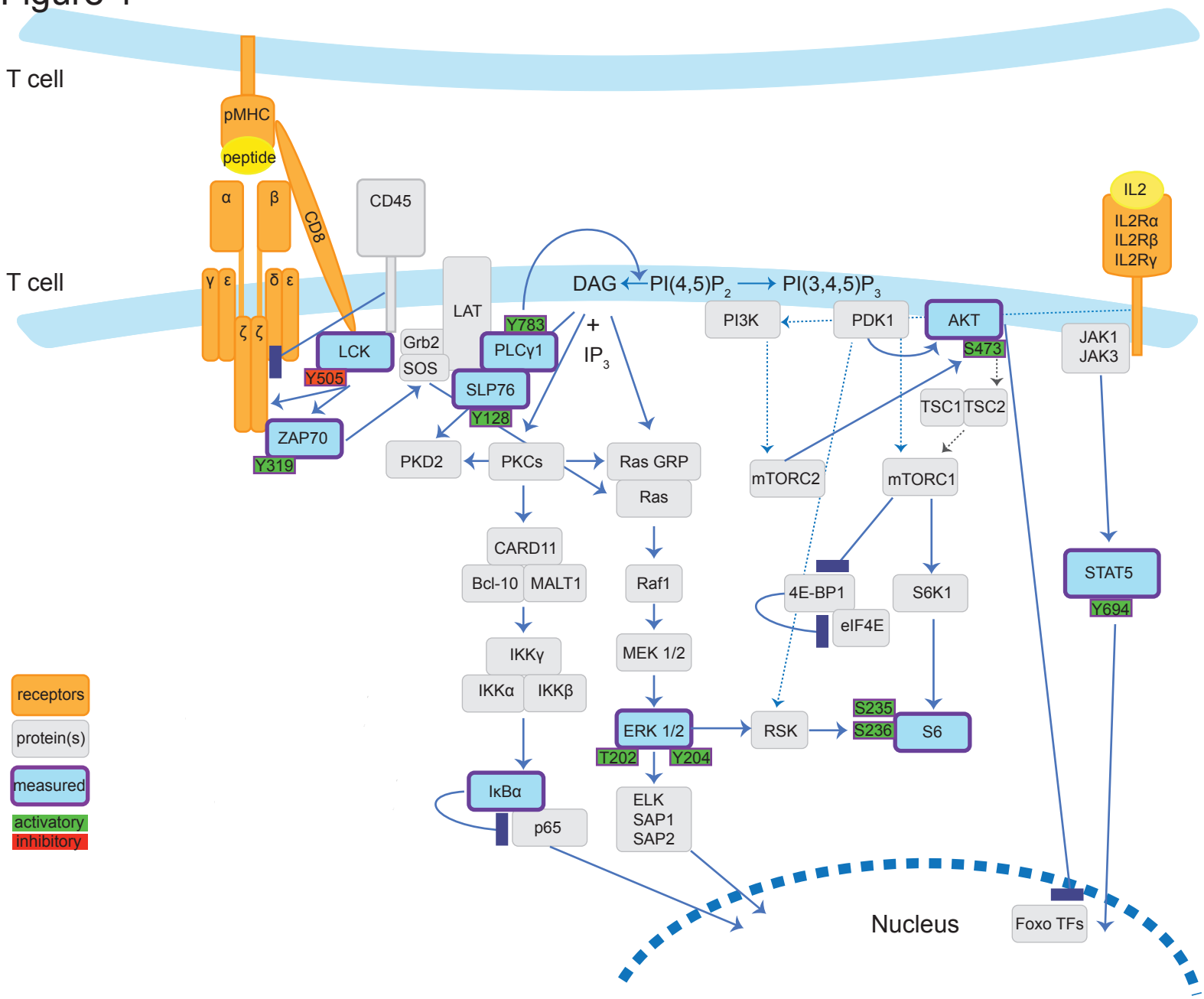
T cell
T cell
pMHC
peptide
α
β
CD8
γ
ε
δ
ε
ζ
ζ
CD45
LAT
Y783
PLCγ1
+
IP3
DAG
PI(4,5)P2
PI(3,4,5)P3
PI3K
PDK1
AKT
S473
IL2
IL2Rα
IL2Rβ
IL2Rγ
JAK1
JAK3
LCK
Y505
Grb2
SOS
SLP76
Y128
ZAP70
Y319
TSC1
TSC2
PKD2
PKCs
Ras GRP
Ras
mTORC2
mTORC1
CARD11
Bcl-10
MALT1
Raf1
4E-BP1
eIF4E
S6K1
STAT5
Y694
IKKγ
IKKα
IKKβ
MEK 1/2
ERK 1/2
T202
Y204
RSK
S235
S236
S6
IκBα
p65
ELK
SAP1
SAP2
Nucleus
Foxo TFs
receptors
protein(s)
measured
activatory
inhibitory

Figure 2

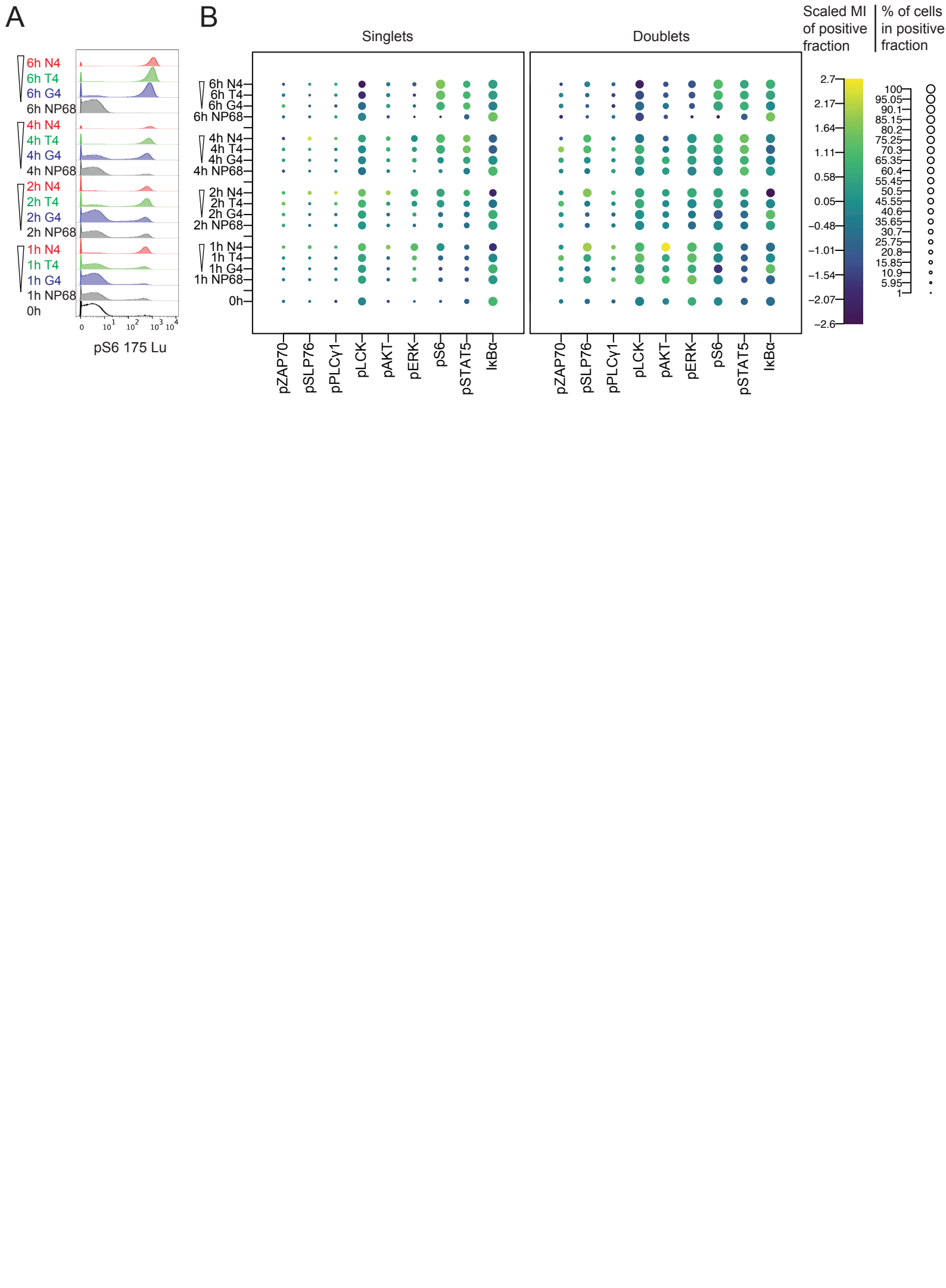
A
6h N4
6h T4
6h G4
6h NP68
4h N4
4h T4
4h G4
4h NP68
2h N4
2h T4
2h G4
2h NP68
1h N4
1h T4
1h G4
1h NP68
0h
pS6 175 Lu
B
Singlets
Doublets
Scaled MI of positive fraction
% of cells in positive fraction
pZAP70
pSLP76
pPLCγ1
pLCK
pAKT
pERK
pS6
pSTAT5
IκBα

Figure 3

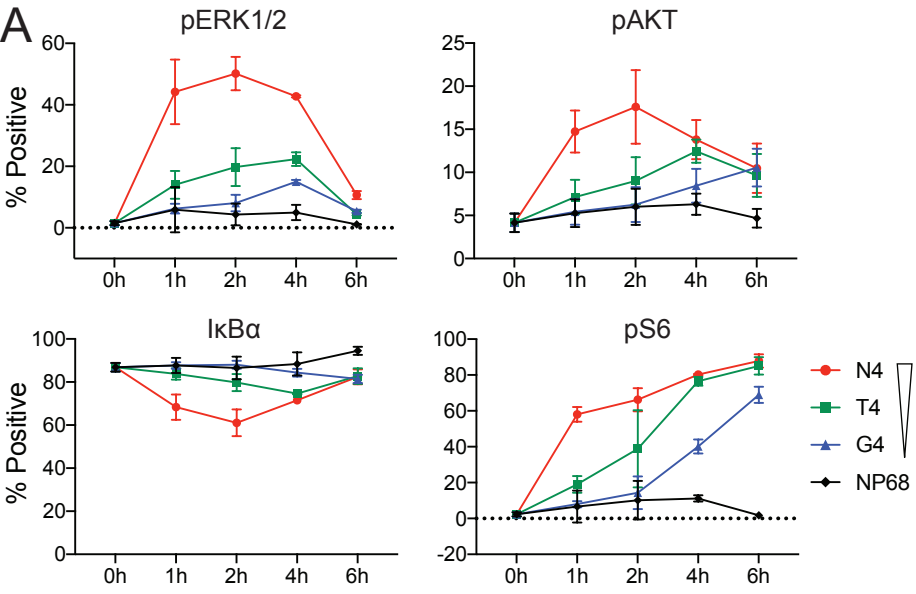
A
pERK1/2
pAKT
IκBα
pS6
% Positive
0h
1h
2h
4h
6h
N4
T4
G4
NP68

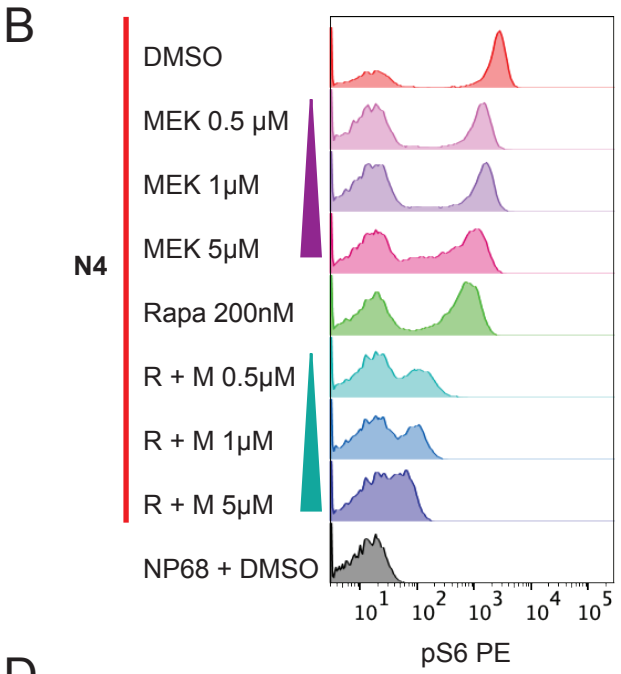
B
N4
DMSO
MEK 0.5 μM
MEK 1μM
MEK 5μM
Rapa 200nM
R + M 0.5μM
R + M 1μM
R + M 5μM
NP68 + DMSO
pS6 PE

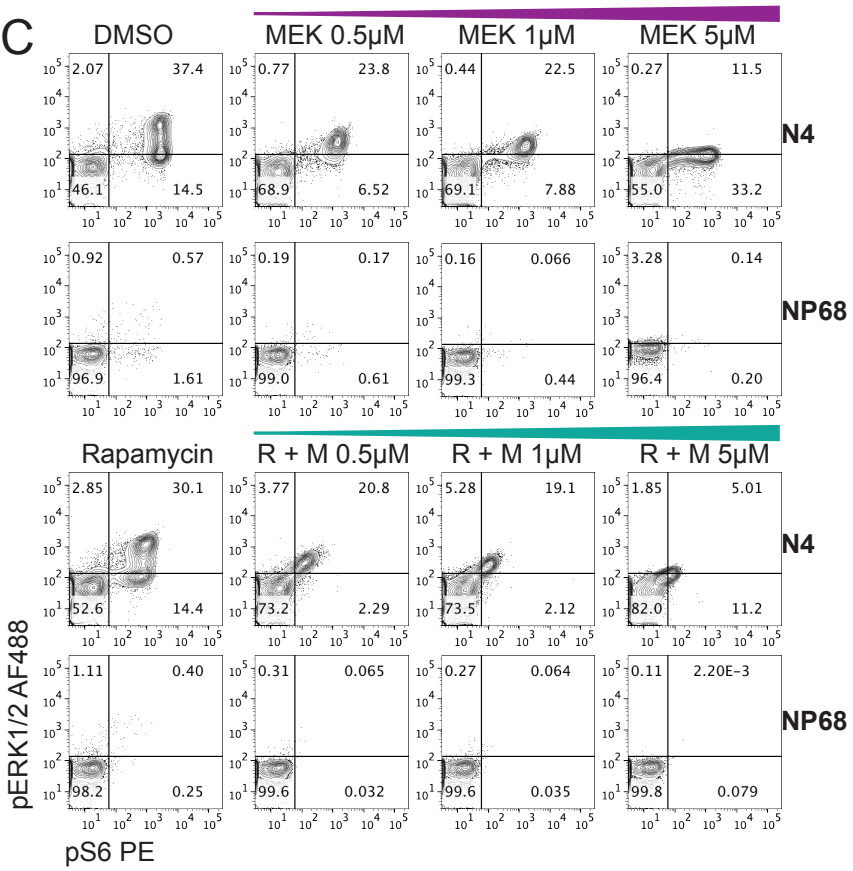
C
DMSO
MEK 0.5μM
MEK 1μM
MEK 5μM
Rapamycin
R + M 0.5μM
R + M 1μM
R + M 5μM
N4
NP68
pERK1/2 AF488
pS6 PE

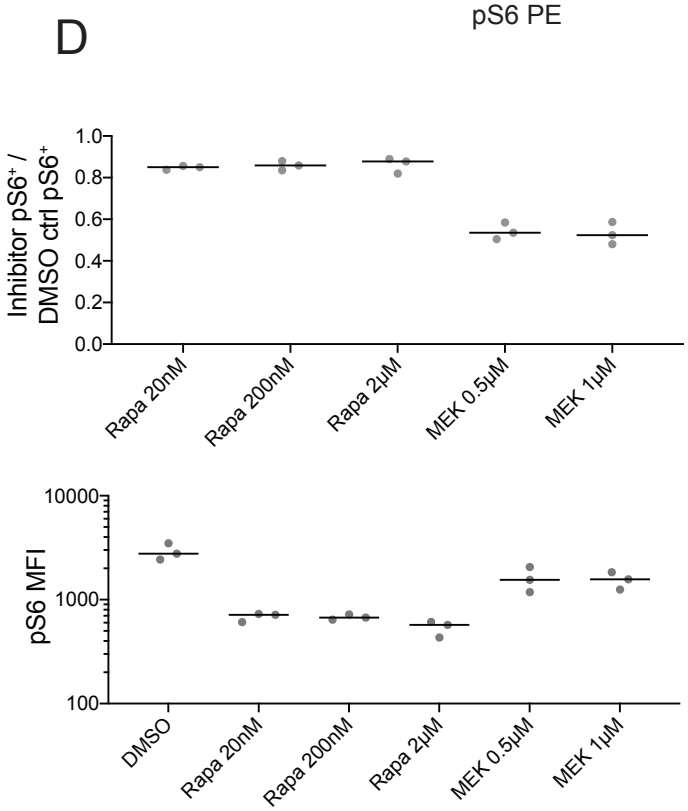
D
Inhibitor pS6+ / DMSO ctrl pS6+
Rapa 20nM
Rapa 200nM
Rapa 2μM
MEK 0.5μM
MEK 1μM
pS6 MFI
DMSO

Figure 4

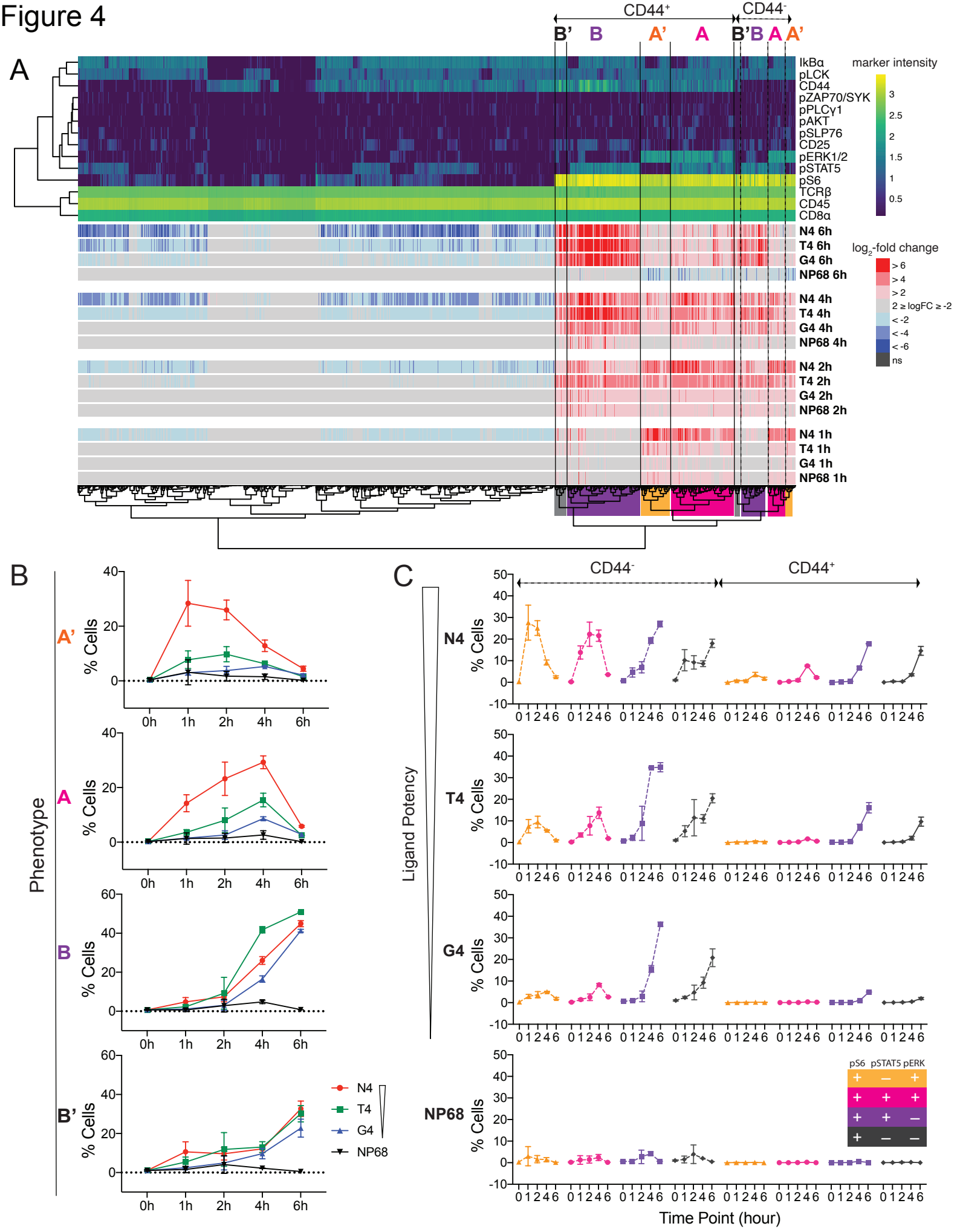
A
CD44+
CD44-
B' B A' A B' B A A'
IkBα
pLCK
CD44
pZAP70/SYK
pPLCγ1
pAKT
pSLP76
CD25
pERK1/2
pSTAT5
pS6
TCRβ
CD45
CD8α
marker intensity
3
2.5
2
1.5
1
0.5
N4 6h
T4 6h
G4 6h
NP68 6h
N4 4h
T4 4h
G4 4h
NP68 4h
N4 2h
T4 2h
G4 2h
NP68 2h
N4 1h
T4 1h
G4 1h
NP68 1h
log2-fold change
> 6
> 4
> 2
2 ≥ logFC ≥ -2
< -2
< -4
< -6
ns

B
Phenotype
A'
A
B
B'
% Cells
0h 1h 2h 4h 6h
N4
T4
G4
NP68

C
Ligand Potency
CD44-
CD44+
N4
T4
G4
NP68
% Cells
0 1 2 4 6
pS6 pSTAT5 pERK
Time Point (hour)

Figure 5

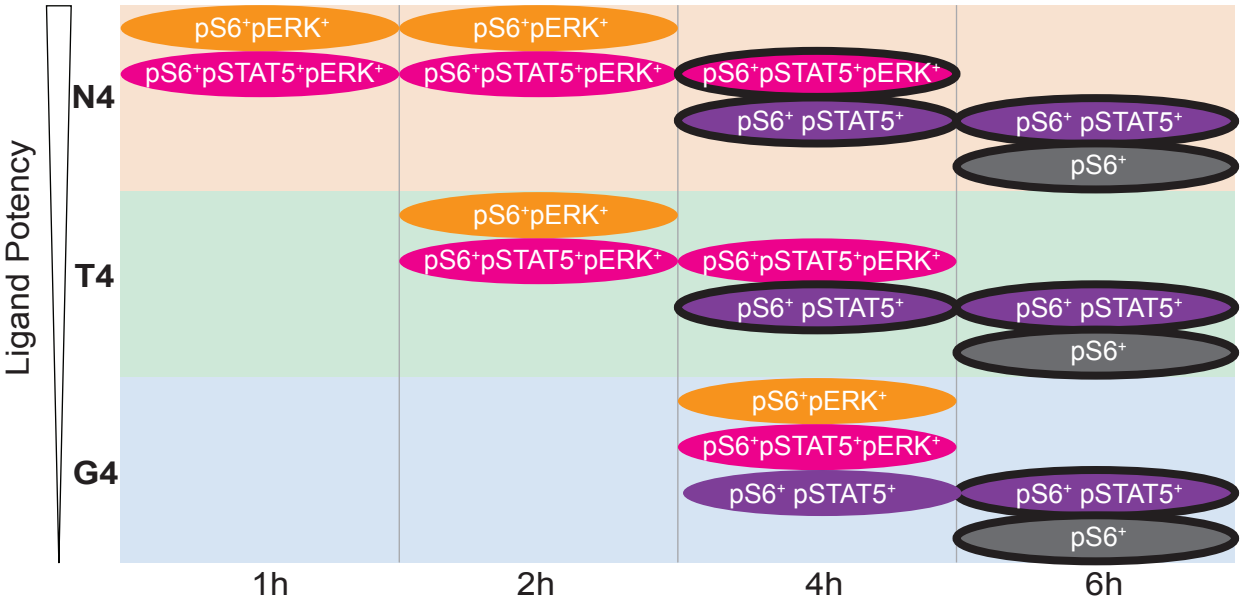
Ligand Potency
N4
T4
G4
pS6+pERK+
pS6+pSTAT5+pERK+
pS6+ pSTAT5+
pS6+
1h
2h
4h
6h

Figure 6

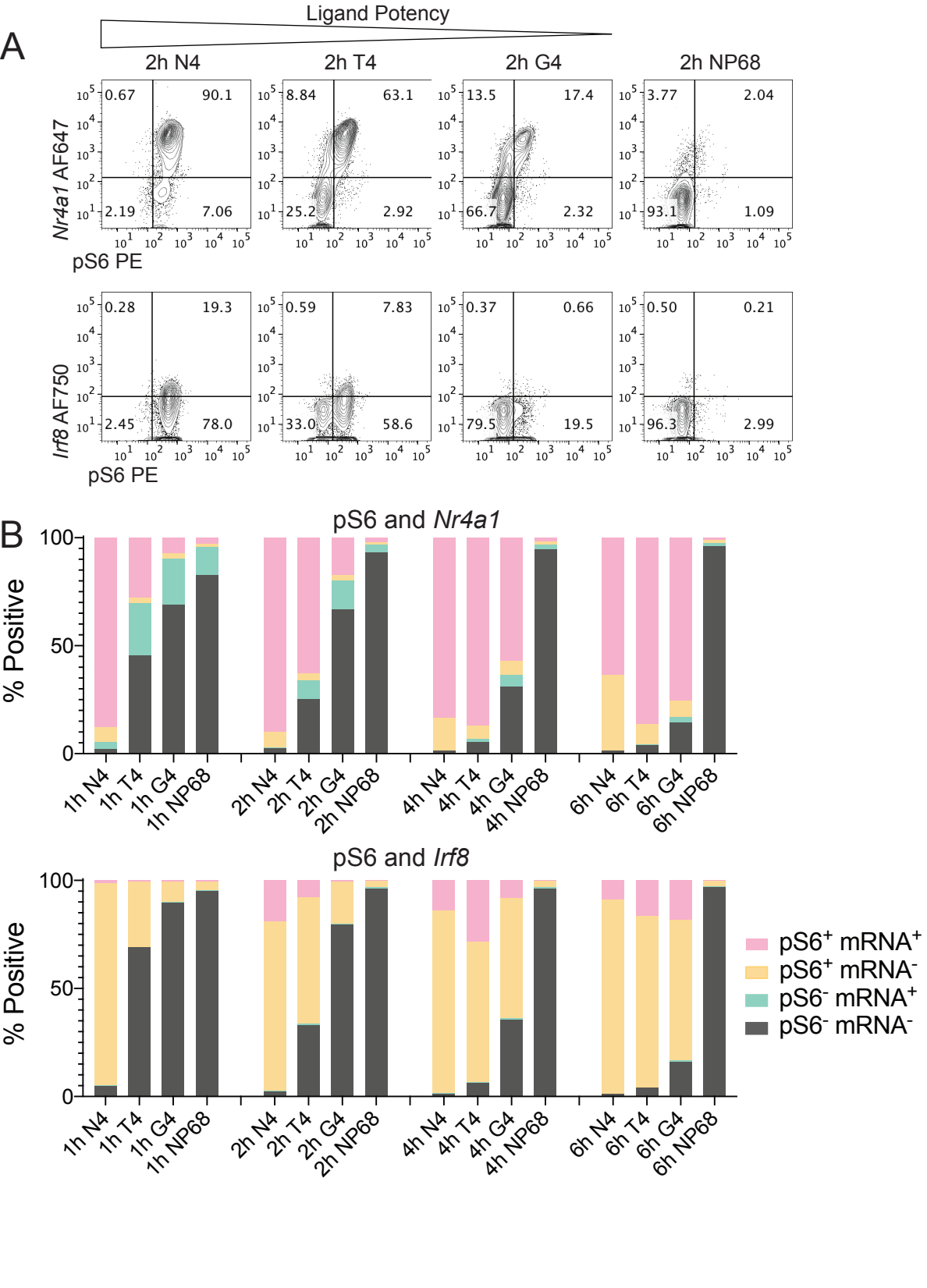
A
Ligand Potency
2h N4
2h T4
2h G4
2h NP68
Nr4a1 AF647
Irf8 AF750
pS6 PE
0.67
90.1
2.19
7.06
8.84
63.1
25.2
2.92
13.5
17.4
66.7
2.32
3.77
2.04
93.1
1.09
0.28
19.3
2.45
78.0
0.59
7.83
33.0
58.6
0.37
0.66
79.5
19.5
0.50
0.21
96.3
2.99
B
pS6 and Nr4a1
pS6 and Irf8
% Positive
100
50
0
1h N4
1h T4
1h G4
1h NP68
2h N4
2h T4
2h G4
2h NP68
4h N4
4h T4
4h G4
4h NP68
6h N4
6h T4
6h G4
6h NP68
pS6+ mRNA+
pS6+ mRNA-
pS6- mRNA+
pS6- mRNA-

Figure 7

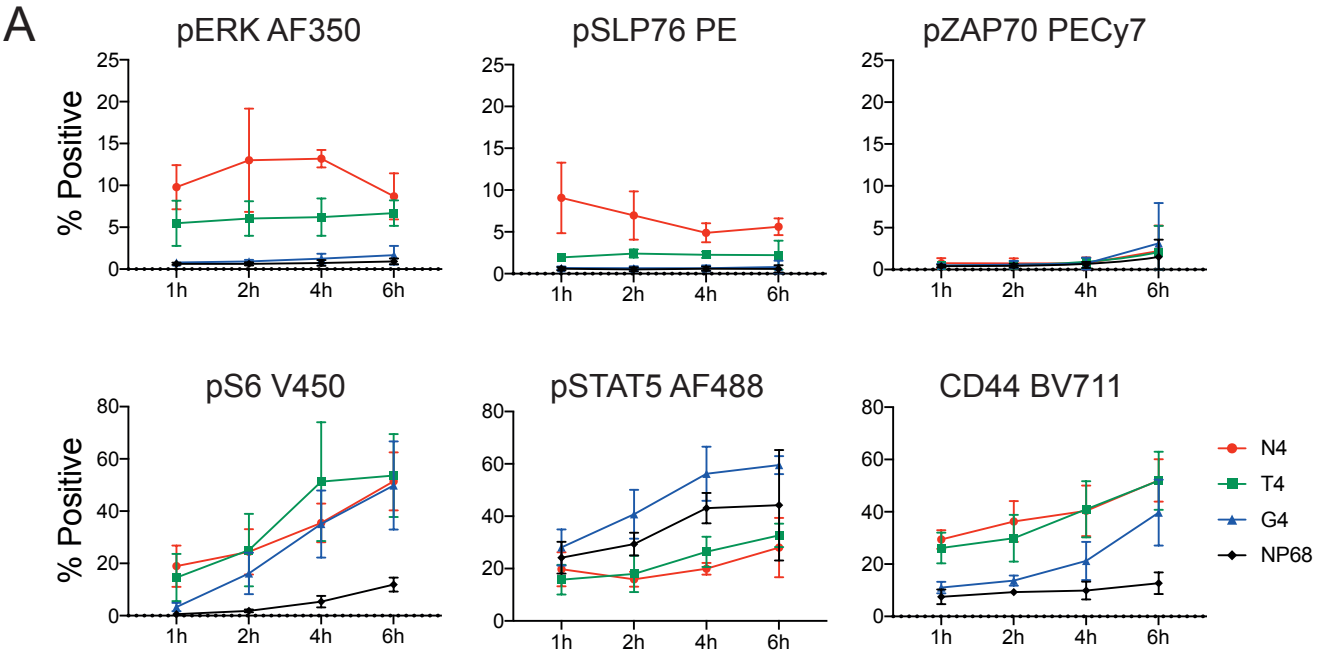
A
pERK AF350
pSLP76 PE
pZAP70 PECy7
pS6 V450
pSTAT5 AF488
CD44 BV711
% Positive
1h
2h
4h
6h
N4
T4
G4
NP68

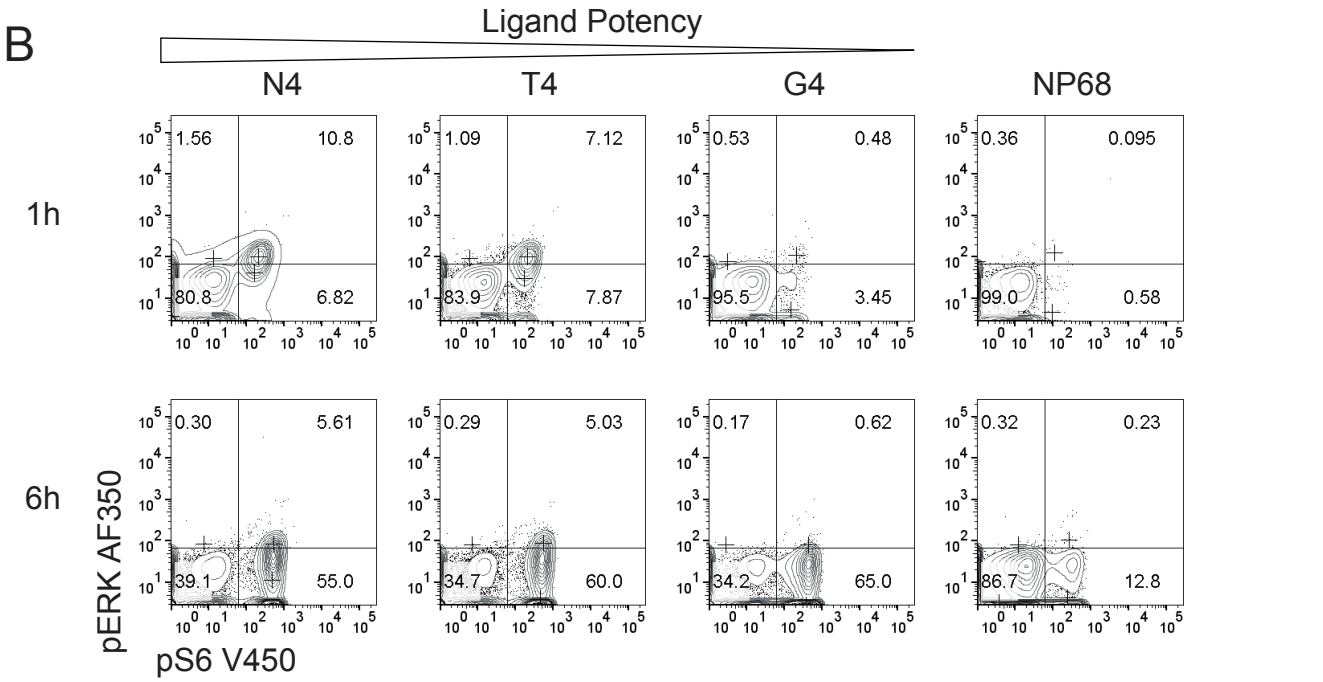
B
Ligand Potency
N4
T4
G4
NP68
1h
6h
1.56
10.8
80.8
6.82
1.09
7.12
83.9
7.87
0.53
0.48
95.5
3.45
0.36
0.095
99.0
0.58
0.30
5.61
39.1
55.0
0.29
5.03
34.7
60.0
0.17
0.62
34.2
65.0
0.32
0.23
86.7
12.8
pERK AF350
pS6 V450

Figure 2 - figure supplement 1

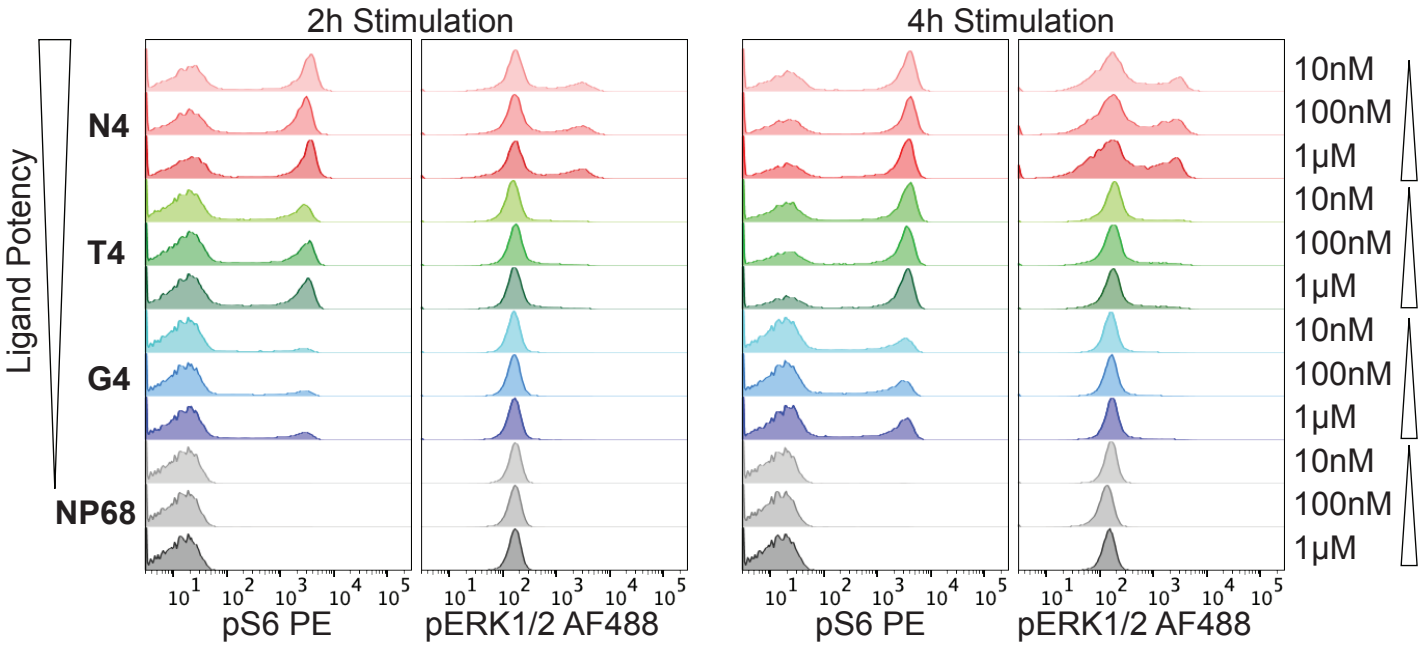

Figure 2 - figure supplement 2

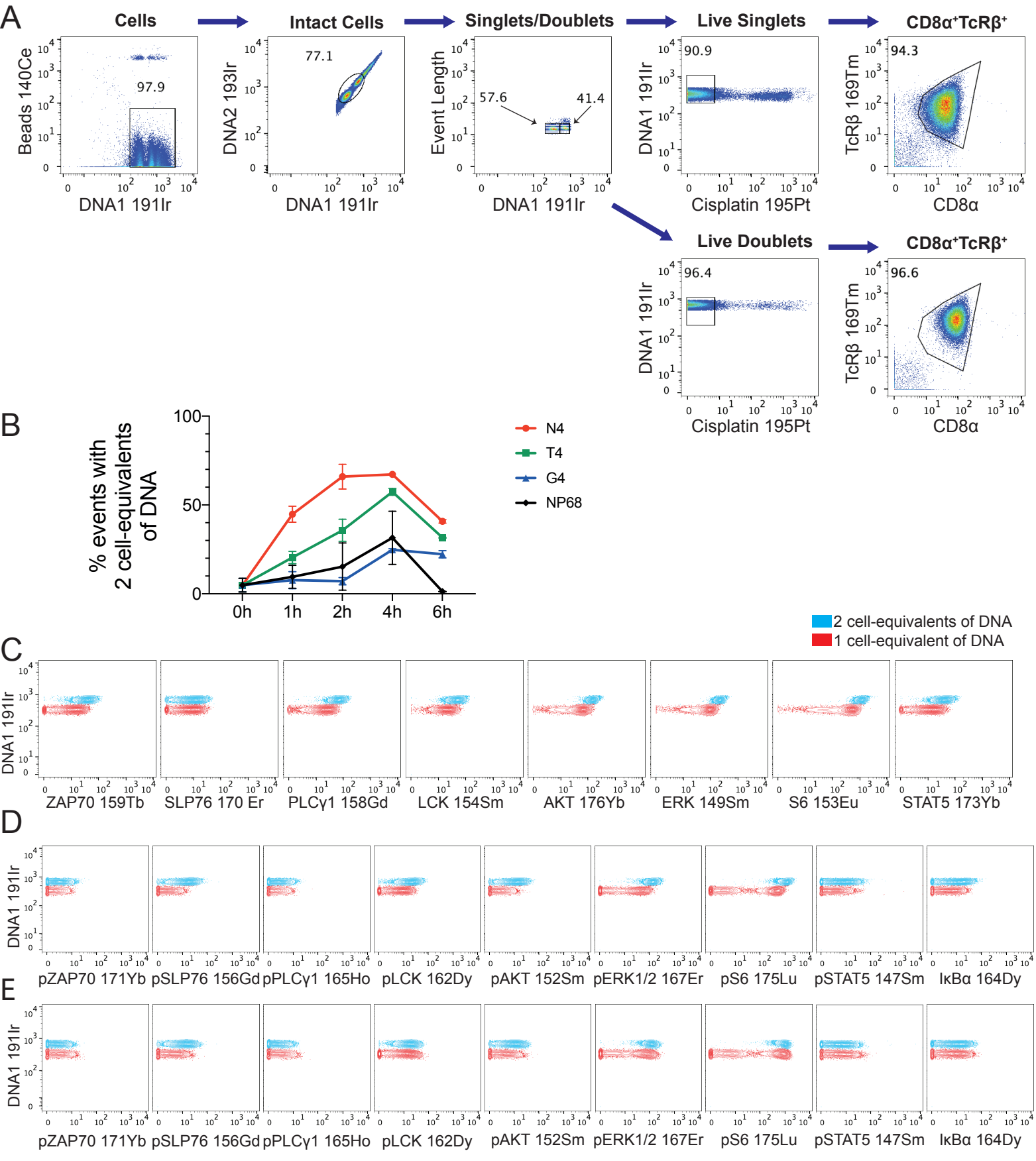

Figure 3 - figure supplement 1

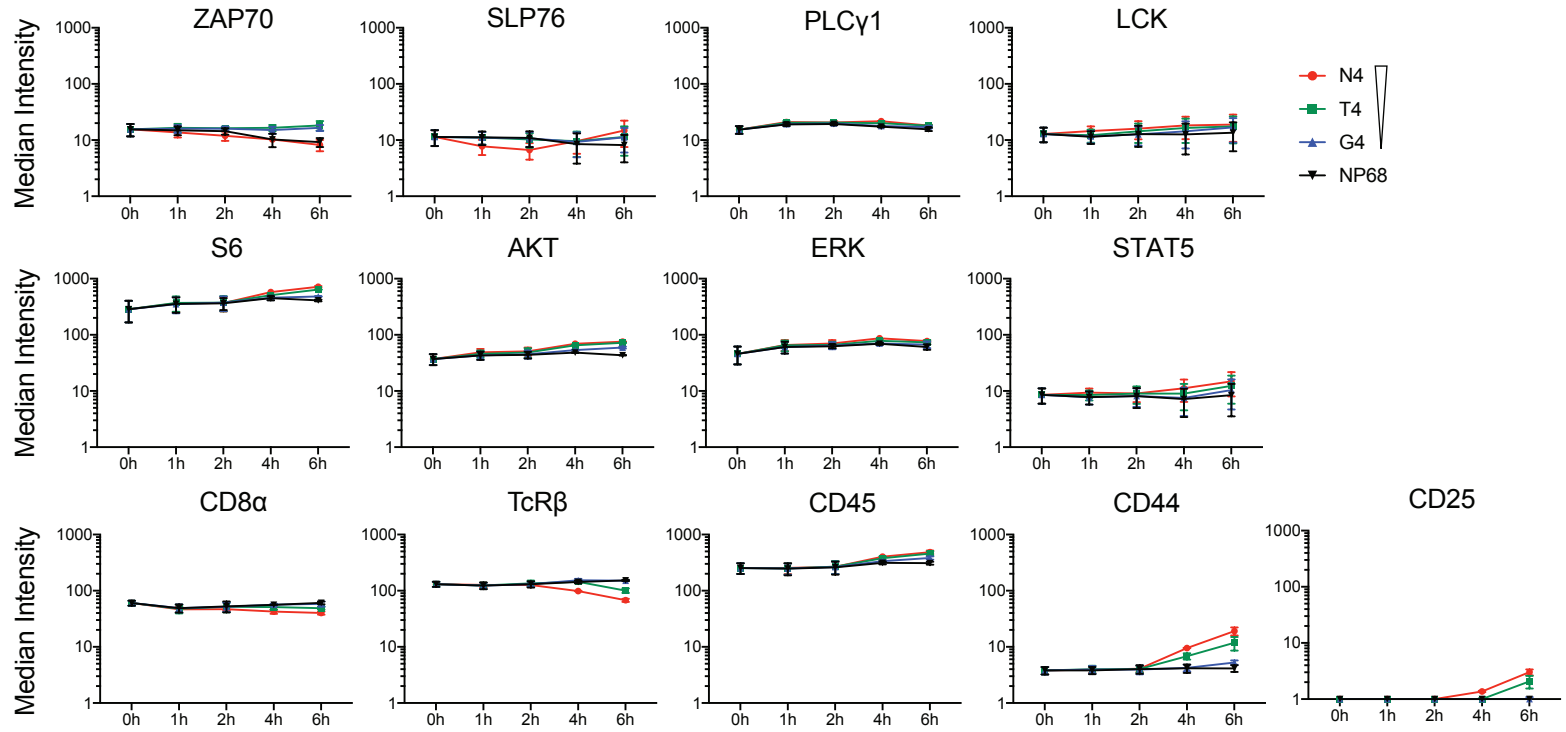

Figure 3 - figure supplement 2

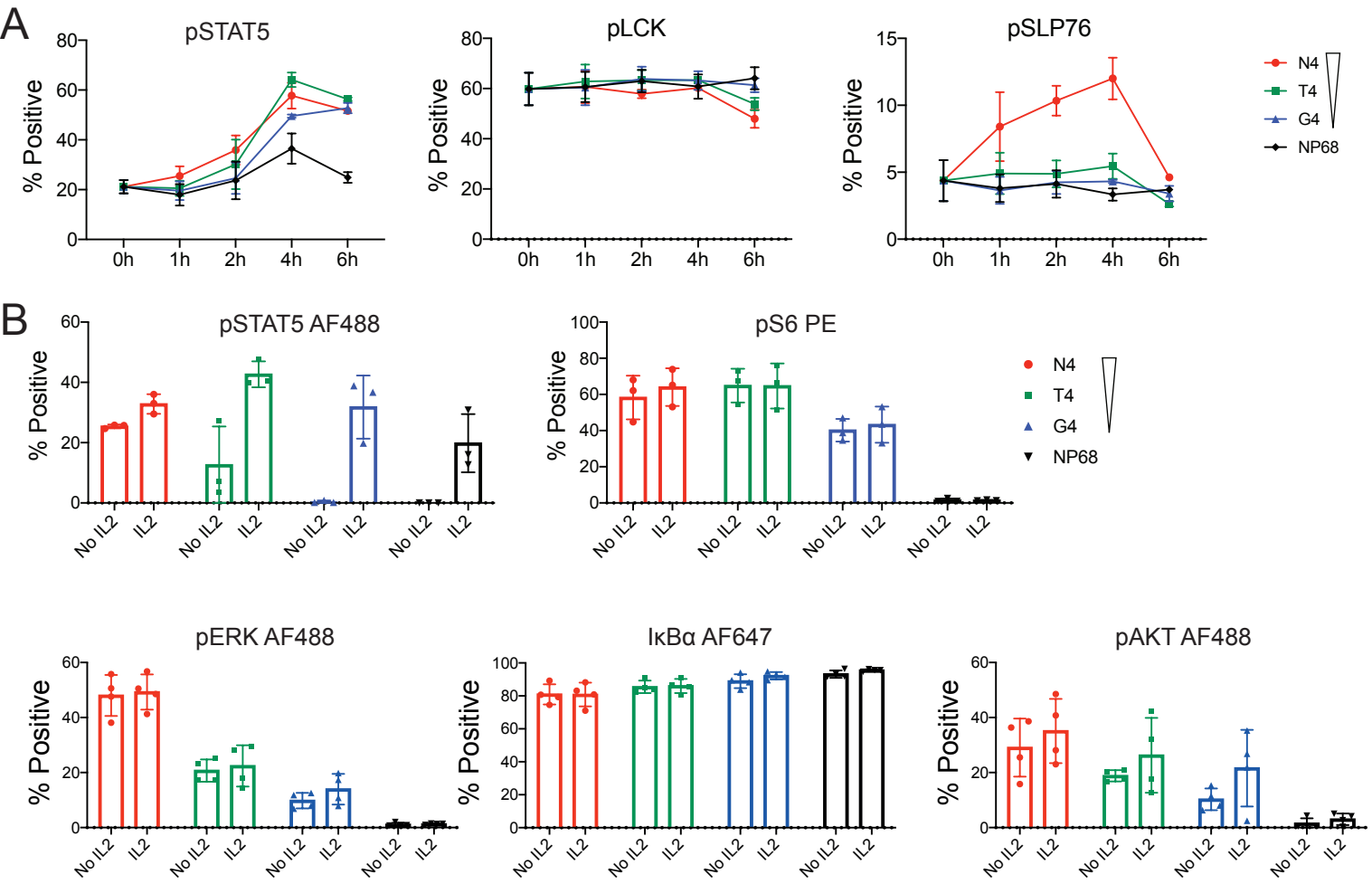

Figure 3 - figure supplement 3

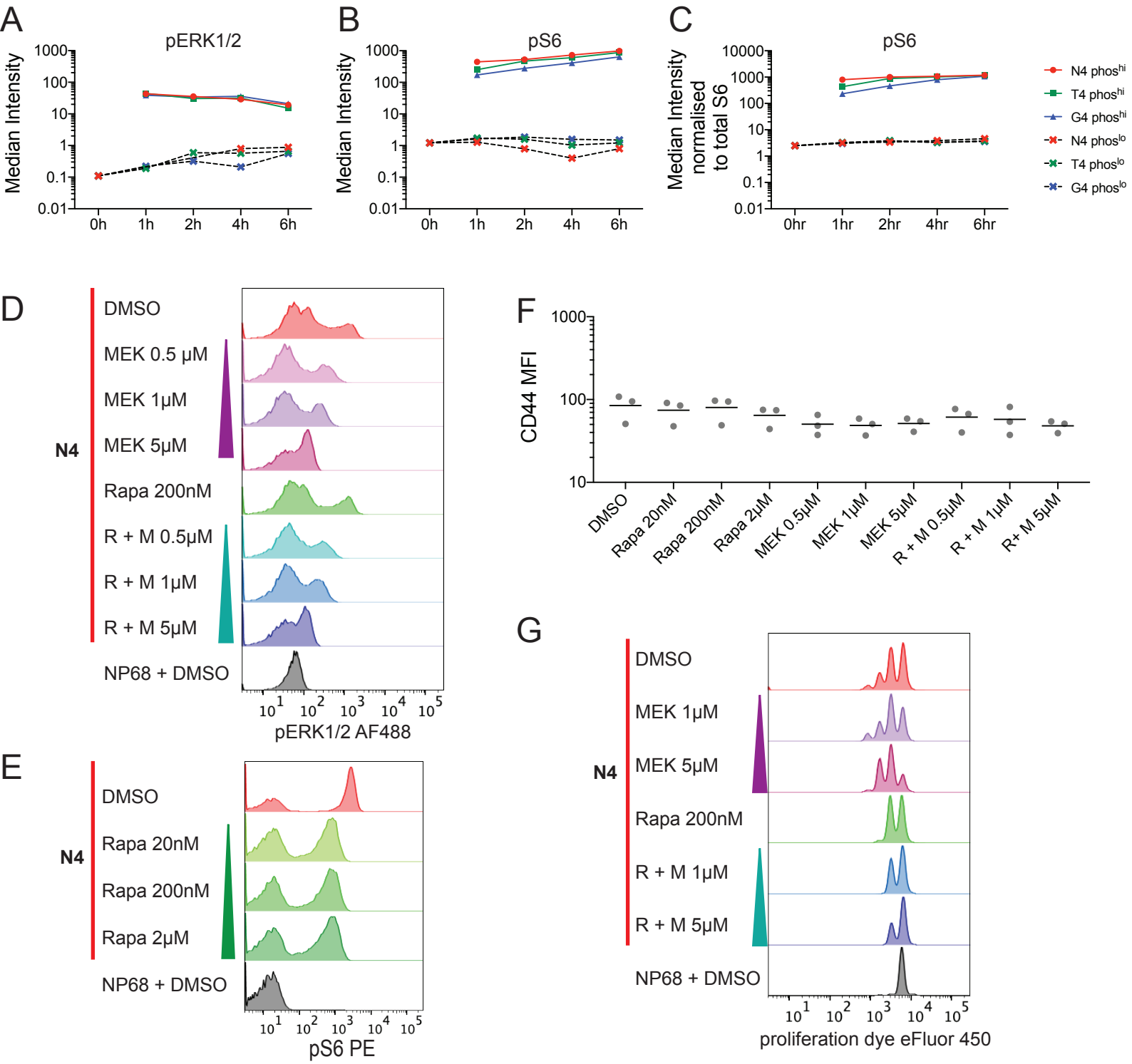

Figure 4 - figure supplement 1

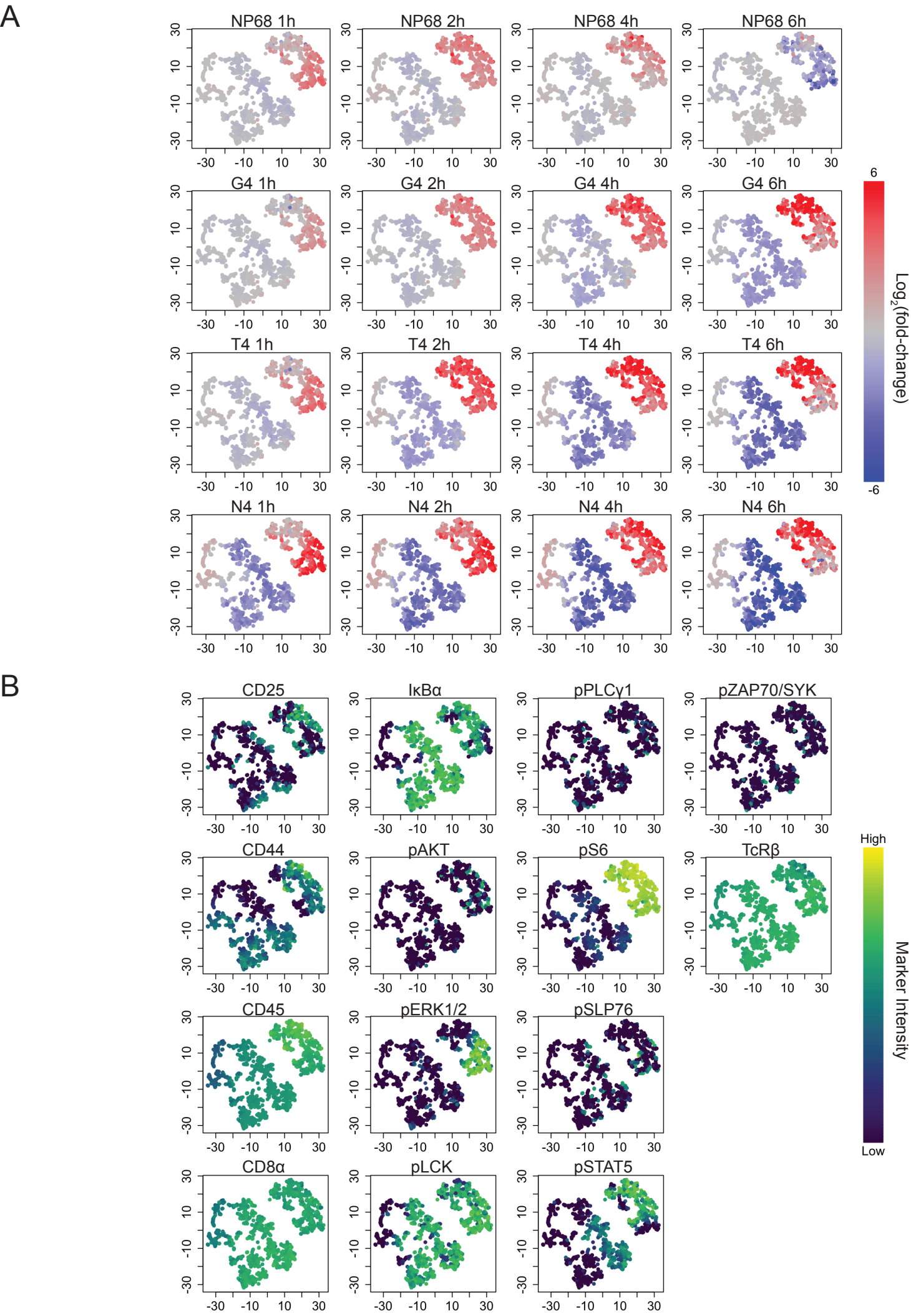

Figure 4 - figure supplement 2

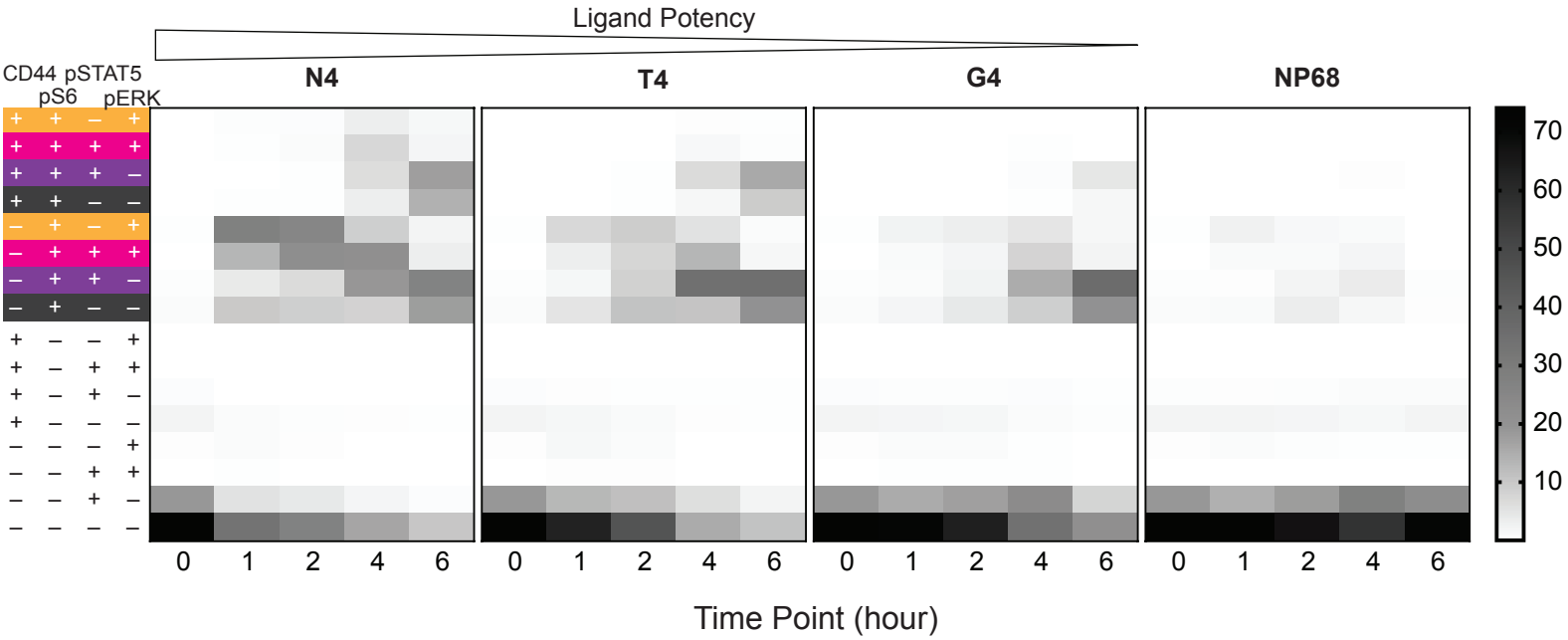

Figure 5 - figure supplement 1

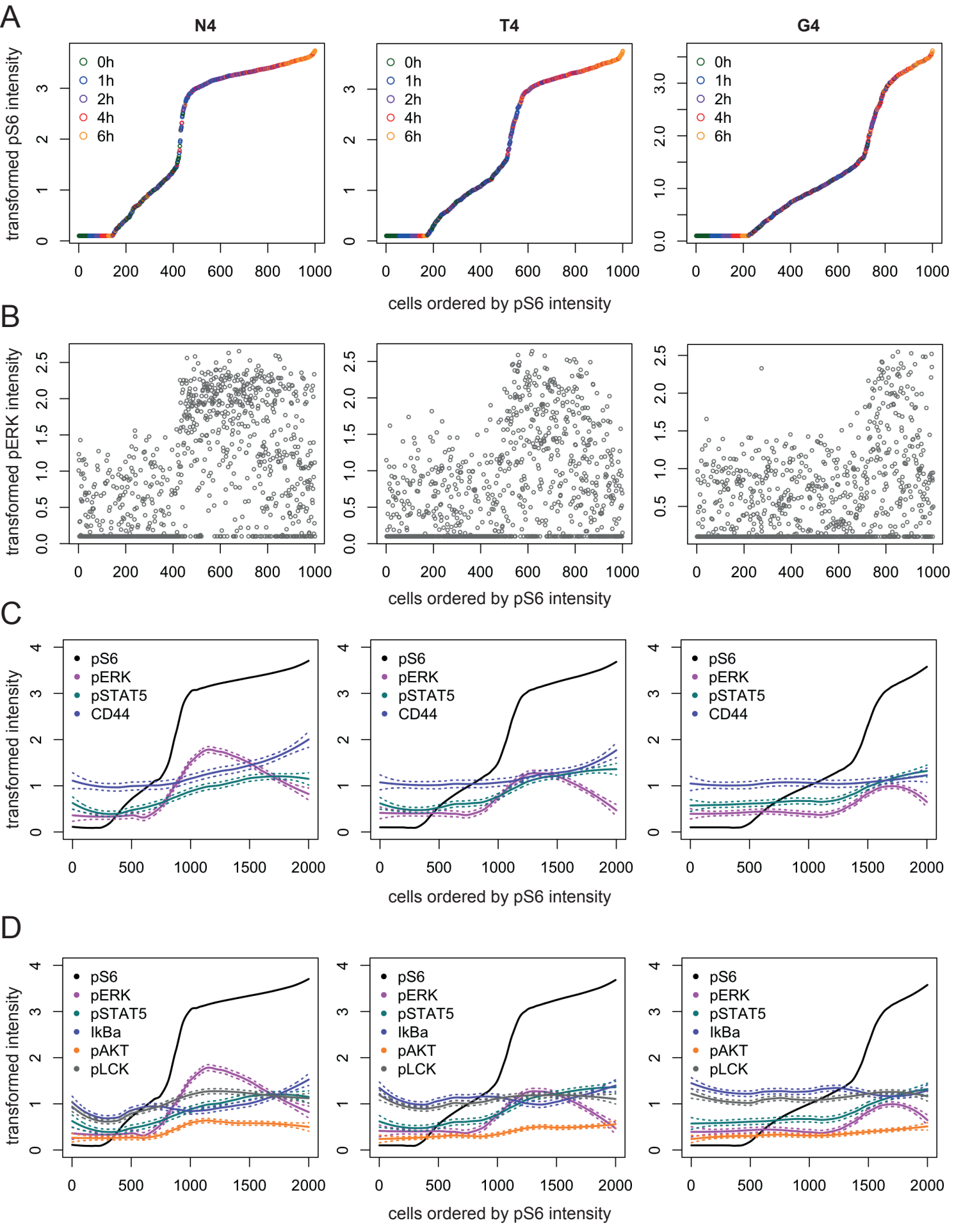

Figure 6 - figure supplement 1

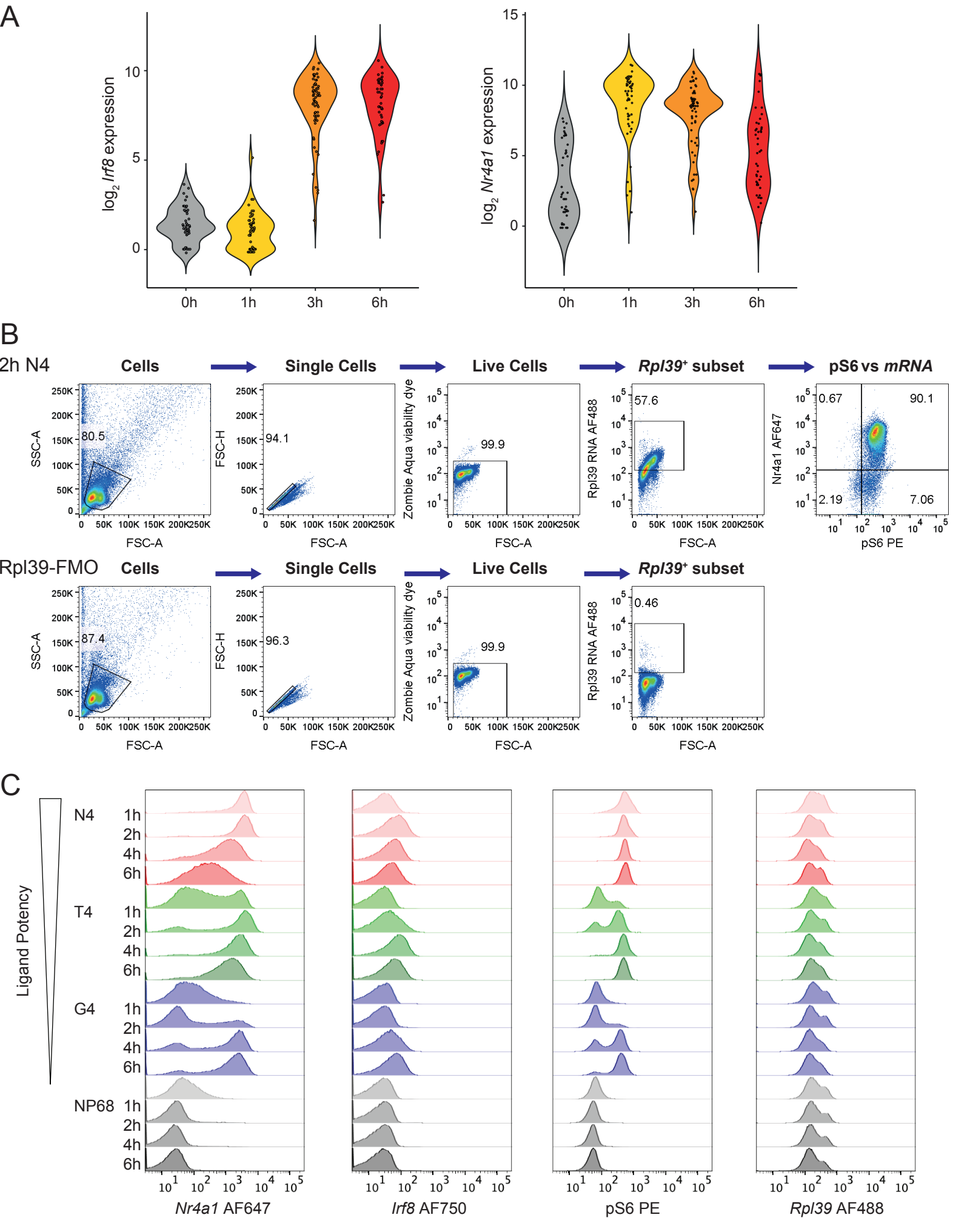

Figure 7 - figure supplement 1